

Dynamical Correlations and Order in Magic-Angle Twisted Bilayer Graphene

Gautam Rai^{1,*}, Lorenzo Crippa^{2,*}, Dumitru Călugăru³, Haoyu Hu,⁴ Francesca Paoletti,² Luca de' Medici⁵, Antoine Georges,^{6,7,8,9} B. Andrei Bernevig,^{3,4,10} Roser Valentí¹¹, Giorgio Sangiovanni^{12,†} and Tim Wehling^{1,12,‡}

¹*Institute of Theoretical Physics, University of Hamburg, Notkestrasse 9, 22607 Hamburg, Germany*

²*Institut für Theoretische Physik und Astrophysik and Würzburg-Dresden Cluster of Excellence ct.qmat, Universität Würzburg, 97074 Würzburg, Germany*

³*Department of Physics, Princeton University, Princeton, New Jersey 08544, USA*

⁴*Donostia International Physics Center, P. Manuel de Lardizabal 4, 20018 Donostia-San Sebastian, Spain*

⁵*LPEM, ESPCI Paris, PSL Research University, CNRS, Sorbonne Université, 75005 Paris France*

⁶*Collège de France, Université PSL, 11 place Marcelin Berthelot, 75005 Paris, France*

⁷*Center for Computational Quantum Physics, Flatiron Institute, 162 Fifth Avenue, New York, New York 10010, USA*

⁸*Centre de Physique Théorique, Ecole Polytechnique, CNRS, Institut Polytechnique de Paris, 91128 Palaiseau Cedex, France*

⁹*DQMP, Université de Genève, 24 quai Ernest Ansermet, CH-1211 Genève, Switzerland*

¹⁰*IKERBASQUE, Basque Foundation for Science, Bilbao, Spain*

¹¹*Institut für Theoretische Physik, Goethe Universität Frankfurt, Max-von-Laue-Strasse 1, 60438 Frankfurt am Main, Germany*

¹²*The Hamburg Centre for Ultrafast Imaging, 22761 Hamburg, Germany*



(Received 28 September 2023; revised 10 April 2024; accepted 8 August 2024; published 11 September 2024)

The interplay of dynamical correlations and electronic ordering is pivotal in shaping phase diagrams of correlated quantum materials. In magic-angle twisted bilayer graphene, transport, thermodynamic, and spectroscopic experiments pinpoint a competition between distinct low-energy states with and without electronic order, as well as between localized and delocalized charge carriers. In this study, we utilize dynamical mean-field theory on the topological heavy fermion model of twisted bilayer graphene to investigate the emergence of electronic correlations and long-range order in the absence of strain. We contrast moment formation, Kondo screening, and ordering on a temperature basis and explain the nature of emergent correlated states based on three central phenomena: (i) the formation of local spin and valley isospin moments around 100 K, (ii) the ordering of the local isospin moments around 10 K preempting Kondo screening, and (iii) a cascading redistribution of charge between localized and delocalized electronic states upon doping. At integer fillings, we find that low-energy spectral weight is depleted in the symmetric phase, while we find insulating states with gaps enhanced by exchange coupling in the zero-strain ordered phases. Doping away from integer filling results in distinct metallic states: a “bad metal” above the ordering temperature, where scattering off the disordered local moments suppresses electronic coherence, and a “good metal” in the ordered states with coherence of quasiparticles facilitated by isospin order. This finding reveals coherence from order as the microscopic mechanism behind the Pomeranchuk effect observed experimentally by Rozen *et al.* [*Nature (London)* **592**, 214 (2021)] and by Saito *et al.* [*Nature (London)* **592**, 220 (2021)]. Upon doping, there is a periodic charge reshuffling between localized and delocalized electronic orbitals leading to cascades of doping-induced Lifshitz transitions, local spectral weight redistributions, and periodic variations of the electronic compressibility ranging from nearly incompressible to negative. Our findings highlight the essential role of charge transfer, hybridization, and ordering in shaping the electronic excitations and thermodynamic properties in twisted bilayer graphene and provide a unified understanding of the most puzzling aspects of scanning tunneling spectroscopy, transport, and compressibility experiments.

DOI: [10.1103/PhysRevX.14.031045](https://doi.org/10.1103/PhysRevX.14.031045)

Subject Areas: Condensed Matter Physics,
Strongly Correlated Materials

*These authors contributed equally to this work.

†Contact author: sangiovanni@physik.uni-wuerzburg.de

‡Contact author: tim.wehling@uni-hamburg.de

Published by the American Physical Society under the terms of the [Creative Commons Attribution 4.0 International license](https://creativecommons.org/licenses/by/4.0/). Further distribution of this work must maintain attribution to the author(s) and the published article's title, journal citation, and DOI.

I. INTRODUCTION

When two layers of graphene are stacked on top of each other with a relative twist angle of 1.1 deg (the magic angle), the emergent long-wavelength moiré pattern gives rise to a band structure with extremely flat bands at the charge neutrality point (CNP) [1–4]. Electronic interaction effects are enhanced in the flat bands, leading to a rich low-temperature phase diagram where superconducting [5–8], insulating [9], correlated metallic [10,11], and exotic magnetic phases [6,12–16] have been observed in experiment by manipulating the charge carrier density. There has been a large theoretical effort toward understanding the insulating [17–78] and superconducting [18–23,79–109] phases, ferromagnetism [49,72–75,110,111], the topological properties [106,112–121], and on constructing suitable models [17,116,118,122–149]. Simultaneously, there has been extensive experimental work [150–180]. For integer fillings, static mean-field approaches such as Hartree-Fock [17,38,39,58,60,61,64] revealed a number of candidate ordered states related by the approximate symmetries of the system that are very close in energy. Depending on filling and the strain and relaxation properties of the sample, these include the time-reversal symmetry breaking Kramer’s intervalley coherent (KIVC) state, valley-polarized (VP) states [17], and incommensurate Kekulé spiral (IKS) states [28,61,64] accompanied by a time-reversal symmetry preserving intervalley coherent (TIVC) order. The near degeneracy of the ordered states suggests that the true state is sample dependent owing to perturbations such as substrate effects, defects, and most importantly strain, in line with recent experiments [71,181].

While the static mean-field approach is suitable for studying the integer-filled case deep in the ordered regime, understanding the temperature-dependent phase diagram, fractional dopings, and the competition of fluctuating local moments and Kondo screening in the symmetric state with isospin polarization in the ordered state requires a dynamic treatment of local correlations. A suitable many-body method for this is dynamical mean-field theory (DMFT) [182–184]. Previous applications of DMFT have successfully investigated the symmetric phase using the Wannier-construction-based multiorbital projector models [185–187] and the topological heavy fermion (THF) model [188], shedding light on Kondo physics and Fermi-surface resetting cascade transitions [156]. Concurrently with the present work, Zhou *et al.* [189] have used DMFT to study an effective single-valley model which imposes one valley to be fully occupied and frozen at all temperatures and all fillings, while the other valley is occupied upon doping without any additional symmetry breaking. These studies focused on fully [185,186,188] (or partially [189]) symmetric states. Therefore, the interplay between dynamic correlations and spontaneous symmetry breaking remains an outstanding question that needs to be addressed.

In this paper, we apply DMFT on a set of symmetry-broken states of unstrained magic-angle twisted bilayer graphene (TBLG)—treating static and dynamic effects on the same footing—and compare the resulting spectral and thermodynamic observables with calculations in the symmetric state. In the symmetric (or interchangeably disordered) state we explicitly suppress long-range order. Our calculations provide a unified understanding of scanning tunneling spectroscopy [156] and compressibility experiments [163,164,190,191], and some puzzling aspects of transport [151,164,192] experiments based on three effects: (i) the formation of local isospin moments around 100 K, (ii) a cascading charge reshuffling between localized and delocalized electronic states, and (iii) the ordering of local isospin moments around 10 K. With our novel charge self-consistent Hartree-Fock+DMFT approach (described in Sec. III), we are able to contrast the temperature scales of moment formation, ordering, and Kondo screening, give quantitative estimates of the ordering temperature on a DMFT level, and provide a *microscopic* theoretical understanding of the temperature- and doping-dependent electronic phase diagram of TBLG. Our approach gives us access to the interacting spectral functions and Fermi surfaces, which link directly to scanning tunneling [7,12,156,181] and quantum twist angle microscopies [193] and lay the basis for an understanding of (magneto)transport experiments and superconductivity in magic-angle twisted bilayer graphene.

In Sec. IV, we apply our findings to a range of observations in the extensive experimental literature on the nonsuperconducting state of TBLG: We provide a microscopic understanding of transport in and around the correlated insulating states, and identify *coherence from order* as the microscopic mechanism behind the *isospin Pomeranchuk effect*. We link cascades in the local density in scanning tunneling spectroscopy and compressibility experiments with Lifshitz transitions, and we provide a proper mathematical treatment of the negative compressibility regions observed in this system. Our main results are summarized below.

At integer fillings in the symmetric state, there is depletion of spectral weight at the Fermi level. In the zero-strain ordered state, there is a hard gap, and the spectral functions are comparable to Hartree-Fock calculations [17]. We find ordering temperatures of ~ 15 K at $\nu = 0, -1$, and ~ 10 K at $\nu = -2$ (where ν measures the number of charge carriers per moiré unit cell with respect to the charge neutrality point). These ordering temperatures are about an order of magnitude lower than the Hartree-Fock prediction, indicating strong suppression of long-range order by local dynamic fluctuations. Upon raising the temperature from ~ 10 K to ~ 100 – 200 K, our DMFT calculations reveal that charge fluctuations are progressively restored—in other words, charge fluctuations are frozen out around the Hartree-Fock ordering temperatures. Above ~ 3 K we find that the local spin susceptibility is

approximately inversely proportional to the temperature. Taken together, the freezing of charge fluctuations and the spin susceptibility point toward a local moment regime spanning the temperature range between the DMFT ordering temperatures (~ 10 K) and Hartree-Fock ordering temperatures (~ 100 K).

We further extend our symmetry-broken calculations to fractional fillings. At small doping away from the insulator, we find a doping-induced insulator-to-metal transition involving the population of coherent light charge carriers. We characterize the Fermi surface across a range of fillings, and find that the topology, the orbital character, and the coherence of the Fermi surface depend on the filling and the absence or presence of long-range order. We identify the changes in the Fermi surface with a sequence of Lifshitz transitions associated with a redistribution of charge between localized and delocalized orbitals. These Lifshitz transitions manifest themselves as the filling-induced cascade transitions seen in compressibility [163,164,191,194] and spectroscopic measurements [156].

Entropy and transport measurements have observed the isospin Pomeranchuk effect in TBLG [151,163,164,192], in a phenomenological analogy to helium-3 [195]. The Pomeranchuk effect has previously been discussed in the solid-state context in the Hubbard model [196,197] and in cold atoms [198,199]. At certain filling fractions, raising the temperature induces a transition from a metallic state (resistivity $\approx 10^{-1}$ k Ω) to a near-insulating state (resistivity $\approx 10^1$ k Ω) at around 5–10 K [164,192]. Our approach allows us to distinguish between two distinct metallic states in TBLG—an order-induced coherent good metal below the DMFT ordering temperature and an incoherent bad metal. Our results therefore point to a microscopic mechanism underlying the observations of “Pomeranchuk physics” in transport and thermodynamics experiments, with good agreement of the temperature scale.

The doping dependencies of the electronic spectra and the existence of disordered moments at temperatures above ~ 10 K is closely linked to the dependence of the chemical potential μ on doping ν in the symmetric phase. Our calculations unveil a balancing mechanism between the filling of the correlated and uncorrelated subspaces, by which the former is progressively occupied with increasing total filling, and the latter is cyclically filled and depleted. We discuss the correlated nature of the system at integer and fractional fillings, showing how, coherently with what is known about the physics of the periodic Anderson model (PAM), Mott-like behavior emerges at integer values of the *total* filling. We compare our DMFT results with the exact solution of the topological heavy Fermion model [17] (see also Sec. II) in the zero-hybridization limit [200] and explain the observed features in the experimentally measurable *charge compressibility*. This is found to exhibit a sawtooth behavior and negative values in extended ranges of dopings, once the geometrical capacitance contribution

is subtracted out analogously to experiments [201–203]. We find that the sawtooth features in the compressibility wash out and the nearly incompressible states fade away at ~ 100 K, which is related to the onset of charge fluctuations. Our observation is consistent with temperature-dependent experimental data [164] and underlines the role of fluctuating local moments in the *cascade transitions*.

II. MODEL

We use the topological heavy fermion model from Ref. [17] to describe the electronic structure of TBLG. This model, derived from the microscopic interacting Bistritzer-MacDonald model [3], connects a set of completely localized f orbitals to highly dispersive c orbitals that carry the topology. Per spin and valley ($\sigma \in \{\uparrow, \downarrow\}$, $\eta \in \{+, -\}$, respectively), there are two f orbitals ($\alpha \in \{1, 2\}$) and four c orbitals [two of each forming the Γ_3 ($a \in \{1, 2\}$) and $\Gamma_1 \oplus \Gamma_2$ ($a \in \{3, 4\}$) representations]. The f orbitals make up most of the flat bands; the exception is at the Γ point in the moiré Brillouin zone, where the flat band character changes to that of the $\Gamma_1 \oplus \Gamma_2$ c orbitals through f - c hybridization. The THF Hamiltonian can be written as

$$\hat{H}_{\text{THF}} = \underbrace{\hat{H}_c + \hat{H}_{cf}}_{\hat{H}_0} + \hat{H}_U + \hat{H}_W + \hat{H}_V + \hat{H}_J. \quad (1)$$

The terms comprising the noninteracting Hamiltonian \hat{H}_0 are \hat{H}_c , which contains the dispersion of the c orbitals, and \hat{H}_{cf} , which contains the hybridization between the two subspaces. \hat{H}_0 defines two important energy scales: the splitting of the $\Gamma_1 \oplus \Gamma_2$ c subspace, $M = 3.7$ meV, which sets the bandwidth of the flat bands, and the f - c hybridization term at Γ , $\gamma = -24.8$ meV, which sets the gap between the flat bands and the high-energy bands. The four terms in the interacting part of the Hamiltonian are \hat{H}_U (\hat{H}_V), the density-density interaction in the f (c) subspace, \hat{H}_W , the density-density interaction between c and f states, and \hat{H}_J , the exchange interaction between the f and c subspaces. They are calculated by performing double-gated Coulomb integrals (see Supplemental Material [204] or Ref. [17] for the definition of each term). Following typical experimental setups, we use a gate distance of 10 nm for the main results of this paper. We have checked that the results are robust within a range of reasonable gate distances and, consequently, a reasonable range of interactions (see Supplemental Material [204]).

In our calculation, we treat \hat{H}_U with DMFT, taking its local many-body effects into account, and the remaining interaction terms via static mean-field decoupling. We perform two sets of calculations: (a) allowing for symmetry-broken states where symmetry breaking in the first iteration is guided by Hartree-Fock results from [17]; (b) in

a fully symmetric state. For later convenience, we define n_f , n_c , and $n = n_f + n_c$ to be the number of f , c , and total electrons per moiré unit cell in the system. The corresponding fillings with respect to the charge neutrality point are given by $\nu_f = n_f - 4$, $\nu_c = n_c - 8$, and $\nu = n - 12$. Because of the exact particle-hole symmetry of the THF model (which may be broken by additional terms not included in this study), the physics at positive and negative ν is related by a particle-hole transformation, and we will limit our discussions to $\nu \leq 0$. In this paper, isospin refers to a generalized spin consisting of electron spin, valley, and orbital degrees of freedom. The corresponding local moments are referred to interchangeably as isospin moments, local moments, and local isospin moments.

III. METHODS

We split the total Hamiltonian into a static and a dynamic part:

$$\hat{H}_{\text{stat}} = \hat{H}_c + \hat{H}_{fc} + \hat{H}_W^{\text{MF}} + \hat{H}_V^{\text{MF}} + \hat{H}_J^{\text{MF}} - 3.5U \sum_{a\eta\sigma} f_{a\eta\sigma}^\dagger f_{a\eta\sigma}, \quad (2)$$

$$\hat{H}_{\text{dyn}} = \frac{U}{2} \sum_{(a\eta\sigma) \neq (a'\eta'\sigma')} f_{a\eta\sigma}^\dagger f_{a\eta\sigma} f_{a'\eta'\sigma'}^\dagger f_{a'\eta'\sigma'}. \quad (3)$$

The superscript MF represents a static mean-field decoupled interaction term (Hartree + Fock for \hat{H}_W^{MF} and \hat{H}_J^{MF} and Hartree for \hat{H}_V^{MF}).

\hat{H}_{stat} plays the role of the lattice Hamiltonian in the DMFT calculation. It must be self-consistently determined as the mean-field decoupled interaction terms depend on the system's density matrix ρ . \hat{H}_{dyn} acts on the f subspace only and induces a frequency-dependent self-energy in the f subspace. We solve the impurity problem with two continuous-time quantum Monte Carlo (CTQMC) hybridization expansion solvers (TRIQS-cthyb [205–207] and w2DYNAMICS [208,209]). We converge two self-consistency loops at once: the DMFT self-consistency condition for the self-energy Σ of the f subspace, and the Hartree-Fock mean-field condition for the total density matrix ρ . Details of the calculations, including the CTQMC parameters and a comparison of TRIQS and w2DYNAMICS results, are given in the Supplemental Material [204] (see also Refs. [210–212] therein). The simulation code [213] and all figure data [214] are publicly available.

The results shown in this paper are obtained for the lowest energy ordered phases predicted by a Hartree-Fock analysis [17] of the THF model in the absence of strain. At the charge neutrality point ($\nu = 0$), both spin sectors are half filled with KIVC order. Upon hole doping once ($\nu = -1$), one spin sector is KIVC ordered, while the other spin sector is valley polarized, and at half filling ($\nu = -2$), one spin sector has KIVC order, while the other

has no long-range order. We emphasize that these states and their flat- and chiral-U(4) related counterparts valley-polarized (VP) and intervalley-coherent (TIVC) states are very close in energy. The true ordered state is therefore sensitive to defects, substrate effects, strain, and other sample-dependent perturbations. These effects can be incorporated with DMFT on the THF model with additional terms, and will be the subject of a future publication. Our goal is to make universal statements about the interplay of correlations and ordering in this system, which likely does not depend on which of the several competing low-temperature ordered phases the system is in.

For the symmetry-broken calculations at integer fillings, we bias the system toward the chosen symmetry-broken solution by applying a weak polarizing field for the first few DMFT iterations, and then turning it off for the remainder until self-consistency is reached. (See Supplemental Material [204] for the definition of the polarizing field.) In the ordered phase, we approach fractional fillings around each integer filling by gradually doping the integer-filling self-consistent solution in small increments.

IV. RESULTS

A. (Nearly) insulating states at integer filling

Figure 1 shows the DMFT spectral functions in the symmetric and the symmetry-broken phases at integer fillings $\nu = 0, -1, -2$. In all cases, the local Hubbard term in \hat{H}_{dyn} shifts the flat band spectral weight of the f subspace away from the Fermi level to form lower and upper Hubbard bands. The remaining low-energy excitations have residual f - and $\Gamma_1 \oplus \Gamma_2$ c -orbital character, while the Γ_3 c -spectral weight remains pushed away to higher energies ($\sim \gamma = 24$ meV) by the f - c hybridization term. We point out two generic differences between the spectral functions in the symmetric [Figs. 1(a)–1(c)] and symmetry-broken [Figs. 1(d)–1(f)] phases. First, the Hubbard bands are relatively sharp in the symmetry-broken phase compared to those in the symmetric phase, indicating that dynamic correlations are weaker in the symmetry-broken phases [215]. Second, while low-energy spectral weight is depleted also in the symmetric state, symmetry breaking supports a robust insulating gap in the absence of strain. This is best seen comparing the momentum-integrated spectral functions in the right-hand panels of Figs. 1(a) and 1(d). In the symmetric case, spectral weight is reduced at the Fermi level but does not vanish. In the ordered case, the spectral weight vanishes and there is a robust gap. This can be understood in the language of the THF model. At the Γ point, the bare (with f - c hybridization turned off) dispersion of the THF model has two contributions at zero energy: Per spin and valley, there is a pair of f orbitals with completely flat bands at zero, and a pair of Γ_3 c orbitals that contribute a pair of particle-hole related parabolic bands touching at zero. f - c hybridization moves

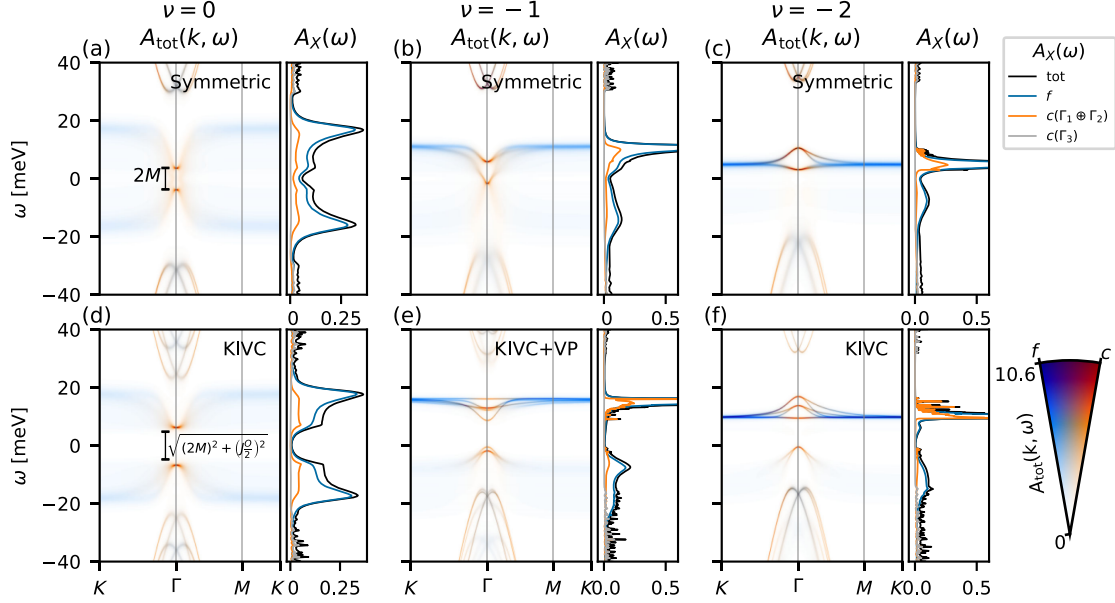


FIG. 1. The momentum-resolved $A(k, \omega)$ and momentum-integrated $A(\omega)$ spectral functions at integer filling in the symmetric (a)–(c) and symmetry-broken phases (d)–(f) at the fillings $\nu = 0, -1, -2$ (from left to right). In the color plot for $A_{\text{tot}}(k, \omega)$, the hue represents the orbital character (blue for f versus red for c) of the spectral weight. The different lines in the $A(\omega)$ plot denote total ($X = \text{tot}$) or orbital-projected [$X = f, c(\dots)$] spectral functions. The data are at 7.7 K.

both of these contributions away from zero to the high-energy bands at the Γ point. Precisely at the Γ point, the flat bands are entirely of $\Gamma_1 \oplus \Gamma_2$ c character. Generically, the c -electron spectral weight is affected by interactions in the f sector directly by the f - c exchange interaction (\hat{H}_J), and indirectly through hybridization effects. The former directly gaps out the c -electron spectral weight near the Fermi level. This is evident in the energy difference between the bright spots in the spectral functions at the Γ point at the CNP in Figs. 1(a) and 1(d). In the symmetric phase [Fig. 1(a)], the $\Gamma_1 \oplus \Gamma_2$ c orbitals retain the $2M$ splitting of the noninteracting Hamiltonian. In the symmetry-broken case [Fig. 1(d)], the splitting gains an additional contribution from the f - c exchange term \hat{H}_J and is given by $\sqrt{(2M)^2 + (OJ/2)^2}$, where O is the off-diagonal intervalley term in the f -subspace density matrix. Note that we treat \hat{H}_J with Hartree-Fock, which neglects any dynamical renormalization effects. Deep in the ordered state, these renormalization effects are expected to be weak. In the symmetric state, it has been shown by poor man’s scaling [216] that the renormalized J is always reduced at low temperatures. Fortuitously, the Hartree-Fock decoupled \hat{H}_J is negligible in the symmetric state—the Fock term vanishes due to its dependence on off-diagonal terms in the density matrix, and the Hartree term is a small ($\sim \frac{1}{8}J$) effective $c - f$ double-counting term.

What is the nature of the (nearly) insulating states at integer fillings? Given the close relation between the THF and the periodic Anderson model, we attempt a classification of insulating states of the THF model in terms of the

phenomenology of the periodic Anderson model. In PAM-like models, different types of insulators including band insulators, Kondo insulators, Mott insulators, and charge-transfer (CT) insulators have been established [217,218].

At integer ν_f , the limit of $U \rightarrow \infty$ corresponds to removing all f states from the THF Hamiltonian. However, without c - f coupling (and thus also without f states at all) the THF model is metallic [17] and not gapped. Clearly, the absence of a gap at $U \rightarrow \infty$ in the symmetric state rules out TBLG at integer filling being a genuine Mott insulator, in agreement with the interpretations of Refs. [185,186]. At the experimentally relevant temperatures of a few kelvin, a Kondo insulator at integer fillings is unlikely, since the f -electron moments are not yet fully screened down to ~ 1 K [188].

The absence of a hard Mott gap can be traced back to a finite t_{fc} in our THF model, similarly to what has been discussed in Ref. [219]: Even at strong interaction strengths, as long as the f electrons can hop into a noninteracting band crossing the Fermi level, a Mott insulator with a clean gap is prevented. The heavy Fermi liquid that replaces it has typically a very low coherence temperature. In accordance with these general expectations (and despite the differences between our model and those of Ref. [219]), we find (see Sec. IV G) that the quasiparticle weight never vanishes in the symmetric state, even close to integer fillings where it is heavily suppressed, displaying the commensurability effects characteristic of incipient Mott phases. Still, in order to see a clean gap, long-range ordering is needed, as we find in our calculations for broken-symmetry states.

The presence of f - and c -spectral weight near the Fermi level is reminiscent of “ p metals” [218] or charge-transfer

insulators [217]. In typical transition metal oxide-based CT insulators like NiO or cuprates [217], the electronic gap is bounded by transition metal $3d$ and oxygen $2p$ -spectral weight from above and below, respectively. The insulating states at $\nu = -2$ with dominantly c -spectral weight below the Fermi level and f -spectral weight above [cf. Figs. 1(c) and 1(f)] resemble this CT scenario. Also, the insulating states $\nu = 0$ and $\nu = -1$ are similar to CT insulators, yet with one decisive difference to the usual CT and p -metal case: In TBLG at $\nu = 0$ and $\nu = -1$ we have delocalized c bands dispersing in between the f -type Hubbard bands from above *and* below. Also differently from the transition metal oxide CT cases, the spectral depletion regions near the Fermi level of TBLG in the symmetric state rely on hybridization between delocalized (c) and localized (f) states. In the ordered states of TBLG, it is the exchange interaction between c and f orbitals leading to mass terms [200] which markedly enhances the gaps in the c sector and thus also the total gaps.

B. Fluctuations and the stability of the ordered solution

Next, we study how doping or raising the temperature affects the ordered states at integer fillings. Figure 2(a) shows the order parameter of the self-consistent solution in a doping-temperature plane generated by gradually doping a particular ordered state at an integer filling. We define the order parameter in the symmetry-broken phase at arbitrary filling by the matrix inner product with the traceless part of the corresponding parent state density matrix (see Supplemental Material [204] and Refs. [220,221] therein). At high enough temperatures, the system flows to the disordered phase under the self-consistency loop. We find the threshold temperature to be ~ 15 K at $\nu = 0, -1$, and ~ 10 K at $\nu = -2$. The ordering temperature predicted by Hartree-Fock is an order of magnitude higher [~ 100 – 150 K; see upper panel of Fig. 2(a)]. Our DMFT simulations show that long-range order is suppressed by local dynamic fluctuations down to about 10 K. Spatial fluctuations, which are neglected in single-site DMFT, are expected to reduce the ordering temperature further. Just below the DMFT ordering temperature, doping away from an integer solution also leads to a disordered solution, resulting in dome-shaped ordered regions as seen in the lower panel of Fig. 2(a). At low enough temperatures, the ordered solution continued from either neighboring integer filling may coexist at a given fractional filling.

The Hartree-Fock ordering temperature encodes the onset of thermally activated charge fluctuations. Above this temperature thermal smearing results in the Hartree-Fock equations converging to the symmetric unpolarized solution. Below this temperature near integer fillings, one charge sector predominantly contributes to the many-body configurations, allowing the formation of local moments (see Supplemental Material [204] for the numerical analysis of the sector statistics). Since Hartree-Fock neglects

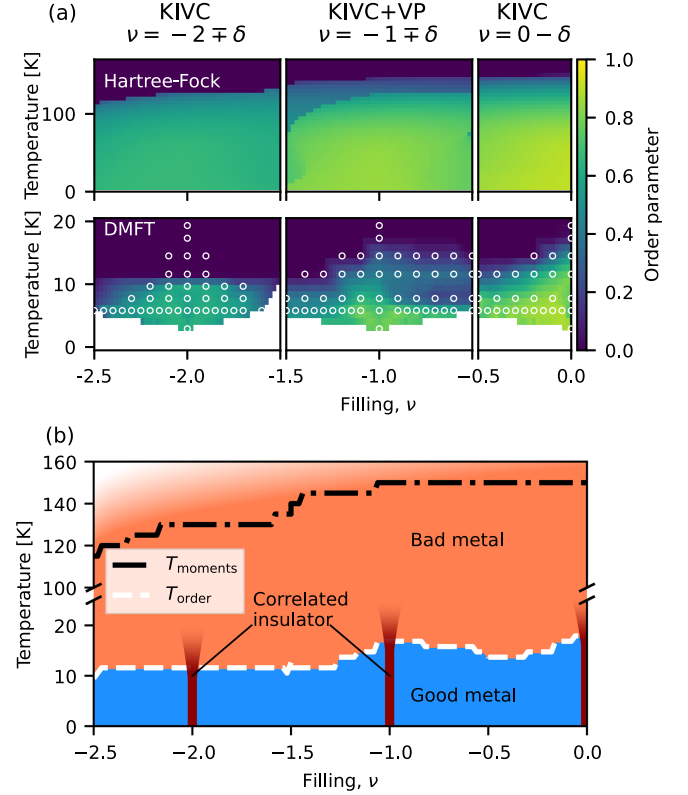


FIG. 2. (a) The magnitude of the symmetry breaking order parameter at various fillings and temperatures. In the bottom panel, white circles represent numerical data points from DMFT simulations at and around the $\nu = -2$ (KIVC), $\nu = -1$ (KIVC + VP), and $\nu = 0$ (KIVC) parent states in the left-hand, middle, and right-hand panels, respectively. The space between circles is filled by linear interpolation. The top panel shows the same quantity from a Hartree-Fock simulation (note the different vertical scale). In the dark blue regions, the self-consistency loop flows to the symmetric state, indicating that the symmetry-broken solution does not exist. (b) A schematic filling-temperature phase diagram. Thermally activated charge fluctuations are frozen below the Hartree-Fock ordering temperature (T_{moments}), allowing local moments to progressively form in the orange region. These local moments order below the DMFT ordering temperature (T_{order}) in the blue region. The DMFT ordering temperature marks the boundary between a bad metal and an order-facilitated good metal at fractional fillings as discussed in Secs. IV E and IV G. The correlated insulators at integer fillings emerging below T_{order} (dark red) fade into the bad metal above T_{order} forming regions with most strongly suppressed quasiparticle weights, cf. Fig. 5(b).

dynamic fluctuations, moments order immediately upon formation. Therefore, the temperature range between the Hartree-Fock and DMFT ordering temperatures is the regime of fluctuating local moments. Correspondingly, in this temperature range, the local spin susceptibility follows the Curie-Weiss law (see Ref. [188] and Supplemental Material [204]). Note that near half-integer filling an intermediate valence regime with quantum charge

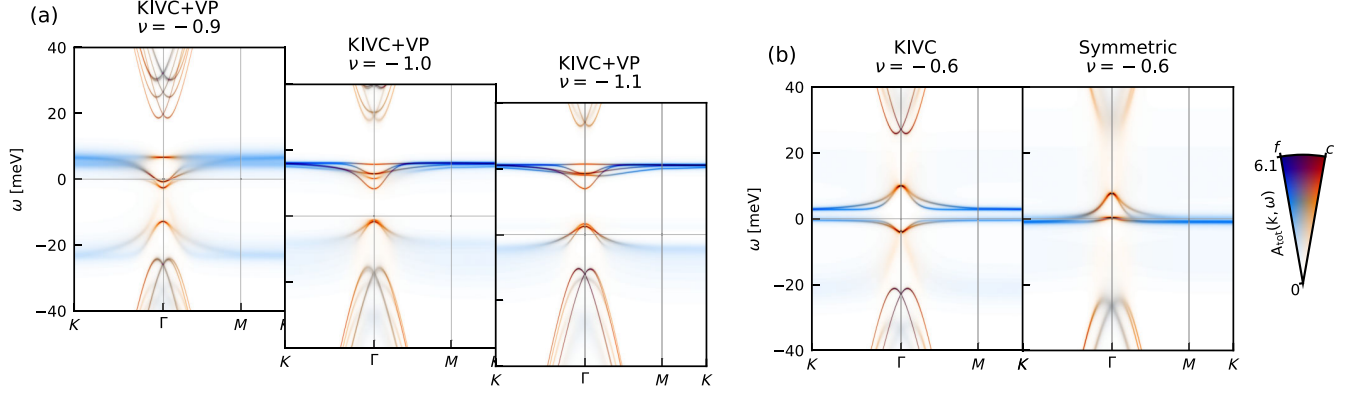


FIG. 3. Spectral functions at 5.8 K (a) at and close to $\nu = -1$ in the ordered phase (b) at $\nu = -0.6$ in the ordered and symmetric phases. In (a), the electron and hole doped panels are shifted such that the Hubbard bands match up with the middle panel. Lightly doping away from an integer-filled insulator moves the Fermi level into the coherent c -spectral weight around the Γ point leading to a coherent metal. Upon further doping as in (b), the Fermi level hits the f part of the flat bands, leading to coherent and incoherent spectral weight at the Fermi level.

fluctuations between two (but not more) neighboring sectors is realized below the Hartree-Fock ordering temperature preventing the identification of well-defined local moments [188], while also additional charge sectors get activated above this temperature scale.

Anticipating the results of Secs. IV C and IV E, where we discuss the metallic states below and above the ordering temperature, we construct a schematic phase diagram in Fig. 2(b). Below the ordering temperature of ~ 10 K, we find an insulator at integer fillings, and a good metal at fractional fillings. The state above the ordering temperature is discussed in Sec. IV E, where we will show that the spectral weight at the Fermi level is generically incoherent, indicating a bad metal. Our results point to a coherence from order at low temperatures, which we expand on in Sec. IV F.

C. Doping-induced insulator-to-metal transition

Away from integer filling, the normal state of TBLG is metallic. The nature of the metallic state depends on the filling and temperature. In fact, we find distinct behaviors upon doping with electron or holes away from the insulators at $\nu = 0$ or $\nu = -1$, on one hand, and $\nu = -2$, on the other hand. In Fig. 3(a), we show how the spectral function changes as we slightly dope the system away from $\nu = -1$ at $T = 5.8$ K in the ordered state with electrons or holes. In this case, we find that the Fermi level moves into the dispersive part of the low-energy bands around the Γ point: The active bands are coherent with delocalized c character. Here, we expect Fermi-liquid-like behavior. Metallic behavior derived from c orbitals on both sides of the insulator points back to the peculiar property of the charge-transfer insulator at $\nu = -1$ with c bands dispersing both above and below. In contrast, the behavior at $\nu = -2$ is asymmetric with respect to doping. Consider the spectral

function in Fig. 1(f). The c part of the upper band is flattened. While hole doping at $\nu = -2$ would lead to metallic behavior just like at $\nu = -1$, electron doping would start to immediately occupy the f orbitals. This is much more reminiscent of a conventional charge-transfer insulator, with localized carriers on one side and delocalized carriers on the other side of the gap.

Upon further doping away from $\nu = -1$ toward $\nu = 0$, the Fermi level eventually also hits the localized f part of the flat bands. This occurs generically once between every two successive integer fillings, and is shown in Fig. 3(b) for $\nu = -0.6$. The Supplemental Material [204] includes a movie showing the evolution of the spectral function as the filling is varied. The ordered phase (in the left-hand panel) has a splitting in the f subspace that is absent in the symmetric phase (in the right-hand panel). This is a consequence of a feedback of the ferromagnetic exchange interaction \hat{H}_J , which is active only in the ordered phase. Because of the isospin order in the f sector, \hat{H}_J behaves like a polarizing field in the c sector, inducing analogous isospin order in the c sector. The induced isospin order in the c sector in turn causes a small polarizing field in the f sector, resulting in the splitting seen in the left-hand panel of Fig. 3(b).

In both the symmetric and ordered state, hitting the localized f part of the spectrum induces a charge reshuffling between the localized and delocalized subspaces, resulting in the sawtooth pattern of orbital-resolved filling seen in Refs. [188,200,222]. This is precisely the region of fillings where experiments see negative compressibilities [164,194]. We discuss the orbital-resolved fillings along with the compressibility further in Sec. IV H. These filling regions are also associated with a sequence of Lifshitz transitions. We identify these Lifshitz transitions with the experimentally observed cascade transitions [156,194] in Sec. IV E.

D. Cascade transitions and signatures of order

In Fig. 4(a), we show the momentum-integrated spectral function as a function of filling in the symmetric and symmetry-broken phases. In both cases, there is a reconstruction of the low-energy spectral features upon changing the doping by an integer value. These are the *cascade transitions* that have been seen experimentally with scanning tunnel spectroscopy (STS) [12,156] and which have been similarly found in the DMFT study of Datta *et al.* [186] for the symmetric state. In the symmetric state, at integer fillings, the spectral function has a two-peak structure, with a lower and an upper peak that are similarly far away from zero, but with their relative spectral weight depending on which integer filling the system is tuned to (for instance, compare $\nu = -2$ and $\nu = -1$ in Fig. 4). Upon hole doping away from an integer filling, the two-peak structure shifts to higher energies, the lower peak merges with a zero-energy resonance, and the upper peak fades away. Upon further hole doping, as the system approaches the next integer filling, the zero-energy resonance shifts to higher energies becoming the new upper peak, and a new lower peak emerges.

The symmetry-broken state behaves the same way except that there is fine low-energy structure, owing to isospin order. The details of the fine structure will depend on the particular ordered state. In particular, the zero-energy peak at fractional fillings, made up primarily of f -spectral weight, is split by a feedback effect from the exchange interaction \hat{H}_J . This splitting is present as long as there is isospin order. See Fig. 2 for the sets of filling and temperature values where this fine structure may be present. Note that our calculation does not include spatial fluctuations, which might further suppress ordering temperatures.

E. Fermiology and Lifshitz transitions

We perform a quasiparticle analysis at the Fermi level to better understand the Fermi surface reconstruction and the Lifshitz transitions underlying the cascades. The exact shape of the Fermi surface will depend on perturbations such as strain, but some general features such as the existence and loose integer-periodic nature of the Lifshitz transitions will remain. We numerically find the zeros, $\hat{H}_{qp}(k)|\psi^i(k)\rangle = 0$, of the quasiparticle Hamiltonian,

$$\hat{H}_{qp}(k) = -\hat{Z}^{1/2} \text{Re}[G^{-1}(\omega + i\epsilon, k)]_{\omega \rightarrow 0} \hat{Z}^{1/2}, \quad (4)$$

where $\hat{Z} = (1 - \partial_{i\omega} \text{Im} \hat{\Sigma}_{\text{tot}}(i\omega)|_{i\omega \rightarrow 0})^{-1}$ is the matrix quasiparticle weight. $\hat{\Sigma}_{\text{tot}}$ is the f -subspace self-energy promoted to the full $f \oplus c$ space by padding with zeros in the c sector (the c sector is treated on a mean-field level and the static contribution to the self-energy is included in the mean-field terms in \hat{H}_{stat}), and the superscript i on $|\psi^i(k)\rangle$ labels the zeros in case there is degeneracy at any k point. The zeros of \hat{H}_{qp} point at potential quasiparticles at the Fermi level.

In particular, the quasiparticle weight \hat{Z} evaluated at the zeros gives information on the coherence of spectral weight at the Fermi level in the form of a k -dependent quasiparticle weight,

$$\frac{1}{Z^i(k)} = \langle \psi^i(k) | \hat{Z}^{-1} | \psi^i(k) \rangle, \quad (5)$$

along a potential Fermi contour. For an uncorrelated Fermi liquid, $Z^i(k) = 1$, and $|\psi^i(k)\rangle$ would give the quasiparticle eigenstates at the Fermi surface. Technical details on the root-finding algorithm used to find $|\psi^i(k)\rangle$ and the rest of the quasiparticle analysis are provided in the Supplemental Material [204].

The blue lines in Figs. 4(b)–4(f), which we henceforth refer to as zero-energy lines (ZELs), mark the location of the zeros $|\psi^i(k)\rangle$ in k space overlaid on the spectral function at the Fermi level in the first moiré Brillouin zone at select fillings. For clarity, the symmetric phase data in Figs. 4(b)–4(d) are projected to the K -valley only. The K' -valley contribution is related by a C_2 rotation. We find that the topology of the ZEL changes with doping. In our zero-strain calculation, between the CNP and $\nu = -1$, we see three regimes. Upon lightly doping away from CNP [Fig. 4(b)], the K -projected ZEL consists of two concentric contours. The three lobes of the outer contour jutting away from the Γ point have low quasiparticle weight, and correspondingly smeared out spectral weight. The inner ring and the inner sections of the outer ring are primarily of c character and more coherent, and form a Fermi contour. Halfway to $\nu = -1$ [Fig. 4(c)], the Fermi level hits the flat f part of the flat band [see also Fig. 3(b)]. This coincides with the concentric ZEL connecting to form a trefoil knot. This ZEL has three points where it intersects itself corresponding to potential Van Hove singularities at the Fermi level. As in the previous case, however, the outer lobes of the ZEL have low quasiparticle weight and are primarily f character. Finally, approaching $\nu = -1$, the ZEL consists of a single closed contour, as seen in Fig. 4(d). We reiterate that the other valley contributes additional 60 deg rotated copies of these Fermi surfaces restoring C_6 symmetry.

In the ordered case, Figs. 4(e)–4(g), the zeros are not valley decoupled as the charge carriers occupy intervalley coherent orbitals. The color map therefore shows the full spectral weight with both valleys included. Generically, away from integer fillings, the zeros are coherent with high quasiparticle weight. The symmetry and topology of the Fermi surface depends on the properties of the active orbital at the chosen filling. Doping with holes away from CNP, the Fermi surface consists of KIVC orbitals getting depleted, resulting in a Fermi surface that is sixfold symmetric. Near $\nu = -1$, there are two occupied KIVC orbitals in one spin sector and an occupied valley-polarized orbital in the other spin sector. Electron (hole) doping corresponds to occupying (depleting) the unoccupied (occupied) valley-polarized orbital, resulting in a Fermi

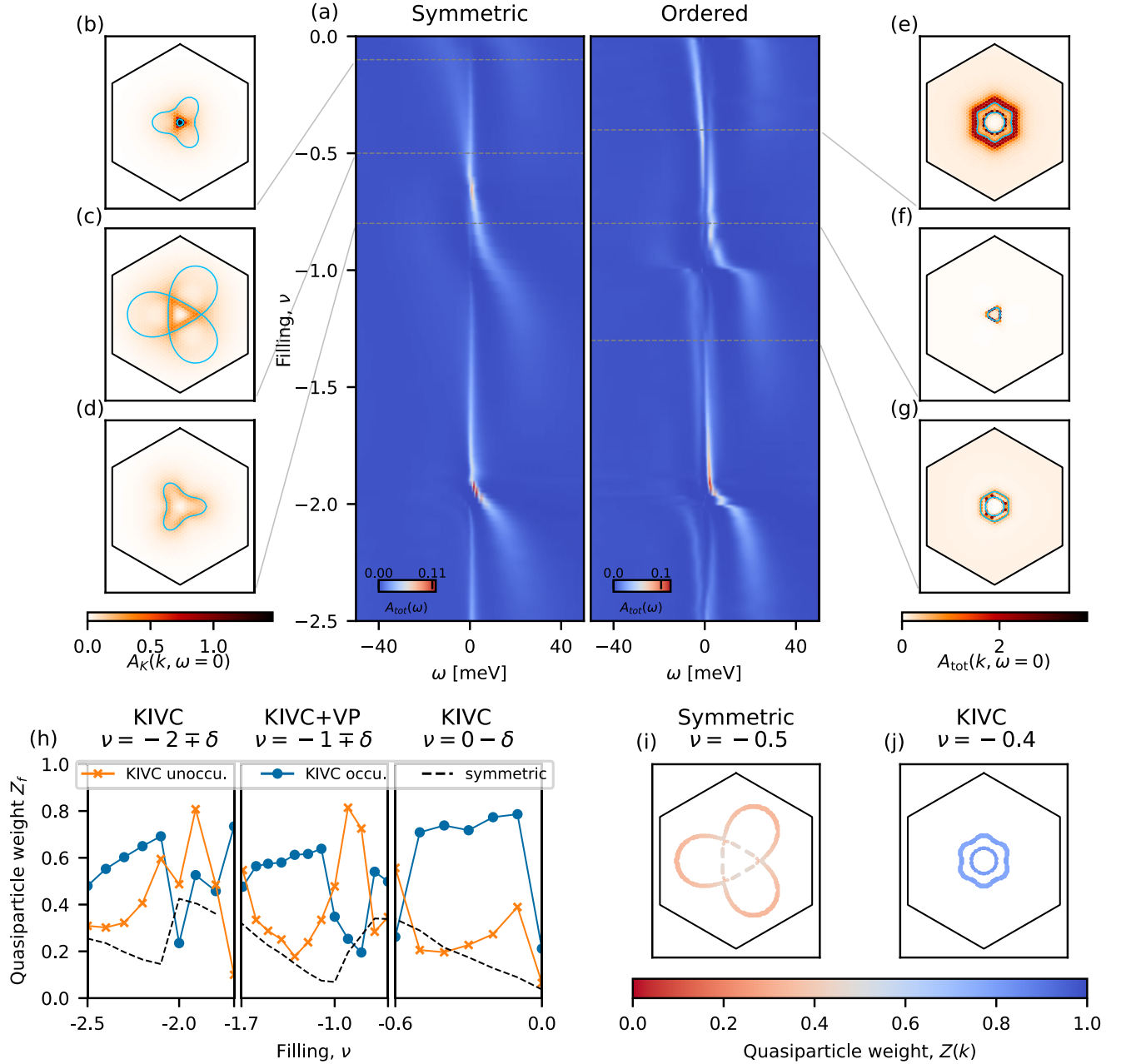


FIG. 4. (a) The momentum-integrated spectral function $A_{\text{tot}}(\omega)$ 5.8 K in the symmetric phase (left) and in the ordered phase (right) as a function of hole doping. The electron doped side (with respect to CNP) is related to the hole doped side by a particle-hole transformation. (b)–(d) The K -valley-projected zero-energy spectral function in the first moiré Brillouin zone in the symmetric phase at select fillings. (e)–(g) The full zero-energy spectral function in the first moiré Brillouin zone in the ordered state at select fillings. The light blue lines mark the zeros of the effective Hamiltonian as identified by a quasiparticle analysis (see main text). (h) A comparison of the f -orbital quasiparticle weight Z_f in the symmetric and ordered states at the same temperature $T = 5.8$ K. In the ordered case, only the spin-up KIVC occupied and unoccupied orbitals are shown for clarity. (i),(j) The quasiparticle weight projected onto the quasiparticle basis along the zeros of the quasiparticle Hamiltonian. All data are at $T = 5.8$ K.

surface that is threefold symmetric. We emphasize that perturbations such as strain will change the details of the ordered state and the shape and symmetries of the Fermi surface. However, there will still be Lifshitz transitions between integer fillings when the Fermi level hits the incoherent f band.

F. Pomeranchuk physics and coherence from order

An important takeaway from Fig. 4 is the different nature of the metallic state in the symmetric and ordered phases. Generically, the spectral weight at the Fermi level in the ordered state originates from much more coherent excitations than in the disordered state. This can be seen from

Fig. 4(h), where we show the quasiparticle weight in the orbital basis over a range of fillings, and from Figs. 4(i) and 4(j), where we show the quasiparticle weight in the quasiparticle basis $Z(k)$ from Eq. (5) at chosen fillings in both the ordered and symmetric phase *at the same temperature*. The quasiparticle weight is clearly higher in the ordered phase than in the symmetric phase, indicating that quasiparticles are more coherent in the ordered state than in the symmetric state *at the same temperature*. Accordingly, the transport and quasiparticle scattering rates (see Supplemental Material [204]) are lower in the ordered phase for most fillings, indicating that there is less scattering than in the symmetric phase, with higher quasiparticle lifetime. Thus, generically at fractional fillings, we expect a good metal in the ordered state and a bad metal in the disordered state. A quantitative analysis of transport is the subject of an ongoing work. With an ordering temperature of about 10–15 K, this interpretation is consistent with transport experiments [151,163,164,192], which observe a sharp drop in resistivity at temperatures below 5–10 K for a range of fillings around the correlated insulating phases. Note that single-site DMFT neglects all spatial fluctuations, which would reduce the ordering temperatures further. With this analysis, we are able to provide a microscopic explanation for the isospin Pomeranchuk effect in TBLG [151,163,164,192]. The bad metal at high temperatures is the result of an incoherent metal stabilized by the isospin entropy of preformed local moments, in analogy to solid helium-3 in the original Pomeranchuk effect [195]. The low-temperature Fermi liquid is a coherent metal induced by spontaneous symmetry breaking. The spectral function in the ordered phase is composed of bands of coherent quasiparticles, which become occupied upon doping away from the insulating states in the close vicinity of integer filling. In this regard, in

contrast to the original Pomeranchuk effect, it is coherence facilitated by order that is responsible for the resistivity drop.

Taken together, our DMFT study reveals the following similarities and differences between the Pomeranchuk physics in He-3 and TBLG. In both systems, disordered fluctuating (iso)spin moments give rise to a high-entropy high-temperature phase. Both in He-3 and TBLG, the (iso) spin entropy is suppressed in the low-temperature state. Both the low-temperature state of TBLG (at noninteger filling) and He-3 can have T -linear Fermi liquid derived contributions to the entropy. Yet, there is a decisive difference between the low-temperature states of TBLG and He-3: In TBLG, the entropy suppression is due to ordering of the (iso)spin moments, while He-3 realizes a Fermi liquid without long-range spin order. In other words, there are no local moments in He-3 at low T , while the isospin moments still exist in TBLG albeit ordered. Hence, the Pomeranchuk physics of TBLG is similar to the coherence from order physics of metallic ferromagnets like SrRuO₃ [223] or relatives of Fe-based superconductors [224].

G. Importance of integer total fillings

Figure 5 reports the filling of the f and c orbitals, as a function of the total filling ν . It is instructive to compare the DMFT solution of the full model with hybridized f and c orbitals to the solution of the zero-hybridization model from Ref. [200]. This is illustrated in Fig. 5(a) where the solid lines refer to the solution with finite hybridization solved with DMFT and the light circles to the zero-hybridization case. It is clear that the model with hybridization obeys a similar energetic balance to the one without hybridization. The c orbitals are periodically filled up and emptied, upon increasing ν . In DMFT, this yields the characteristic, albeit smoothed out, sawtooth behavior.

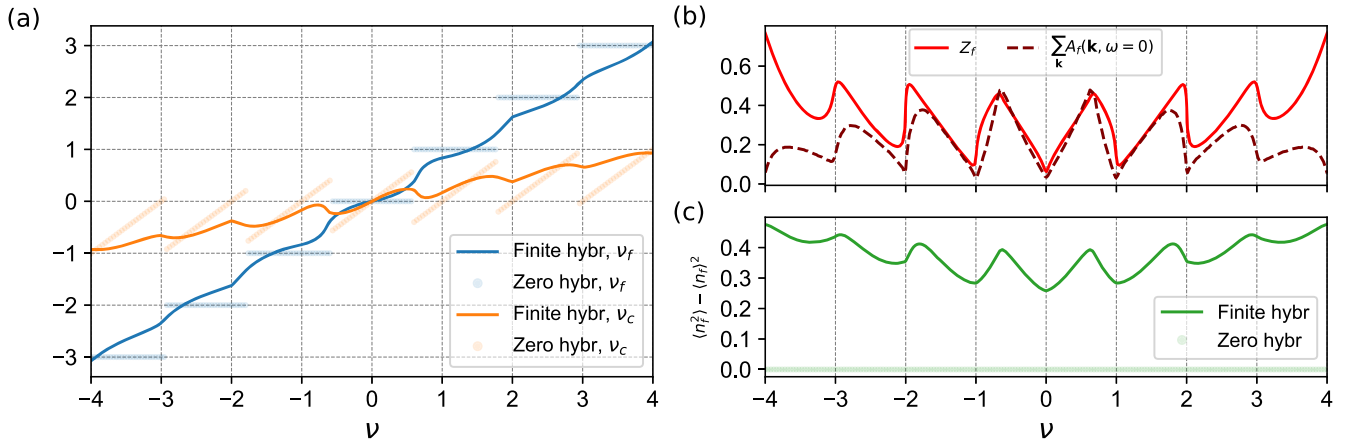


FIG. 5. (a) Partial filling of the f and c orbitals as a function of the total filling ν in the symmetric phase. The dark solid lines show the DMFT results of the full model with hybridization. The light dotted curves are results from the zero-hybridization model solved exactly in Ref. [200]. (b) Quasiparticle weight for the f orbitals, calculated at 11.6 K and the local f -spectral weight at the Fermi level. (c) Charge fluctuations of the f orbitals $\langle n_f^2 \rangle - \langle n_f \rangle^2$ as a function of the total filling ν . Both quantities in (b) and (c) are indicators of the importance in DMFT of the integer values of ν , in contrast to the zero-hybridization solution.

These overall trends displayed by ν_f and ν_c are a consequence of the strong correlations due to the f - f Coulomb terms together with f - c and c - c interactions terms that are present both in the zero-hybridization solution of Ref. [200] and in our DMFT calculation.

There is a further, more fundamental difference between finite and zero hybridization, namely the special role played in the former—and not in the latter—by the integer values of the total filling ν . In the zero-hybridization model, $\nu = -3$, $\nu = -2$, $\nu = -1$, and so on have no special meaning apart from trivially imposing $\nu_c = 0$. On the contrary, the DMFT solution with finite hybridization bears a clear witness of the integer values of the total ν , as evident from Figs. 5(b) and 5(c). The quasiparticle weight of the f orbitals and the local f -spectral weight at the Fermi level, calculated from QMC via the low- T estimator $\sum_{\mathbf{k}} A_f(\mathbf{k}, \omega = 0) = (\beta/\pi) G_f^{\text{QMC}}(\tau = \beta/2)$, display particularly strong variations approaching integer values of ν . At the same time, the fluctuations of the f occupation $\langle n_f^2 \rangle - \langle n_f \rangle^2$ are suppressed near integer values of ν , in contrast to the zero-hybridization case, for which this quantity is flat and vanishes. In the Supplemental Material [204], we show that scattering rate has an analogous strongly filling-dependent behavior. Everywhere apart from the precise fillings at which the cusps in these two quantities occur, the behavior evidenced by these two indicators of the many-body nature of the f electrons reveals a crucial property of the THF model with its full heavy-light fermion hybridization.

Periodic Anderson models ubiquitously show Mott-like behaviors at integer values of the total filling, rather than at integer fillings of the correlated subspace [218,225]. This is independent of whether or not Mott insulating phases are fully realized and is to some extent counterintuitive. One may indeed naively think that the strongest propensity to Mottness is present at integer values of ν_f , not of ν . This “commensurability” physics as a function of total filling is obviously possible only when the hybridization puts the correlated and itinerant subspaces in communication and is captured by DMFT. Indeed, there are two main features that render DMFT especially suited to the task at hand. First, being by construction in the thermodynamic limit it is able to treat integer and fractional fillings on an equal footing. Second, DMFT has been proven to be able to solve models possessing degrees of freedom with different correlation strength in the low-energy subspace (as are f and c orbitals in our case) taking the charge fluctuations occurring between the two fully into account.

H. Compressibility

In Fig. 6 we show the total, f and c fillings as a function of the *intrinsic* chemical potential μ . A discussion on the precise definition of the intrinsic chemical potential and on how the mean-field interaction terms are operationally

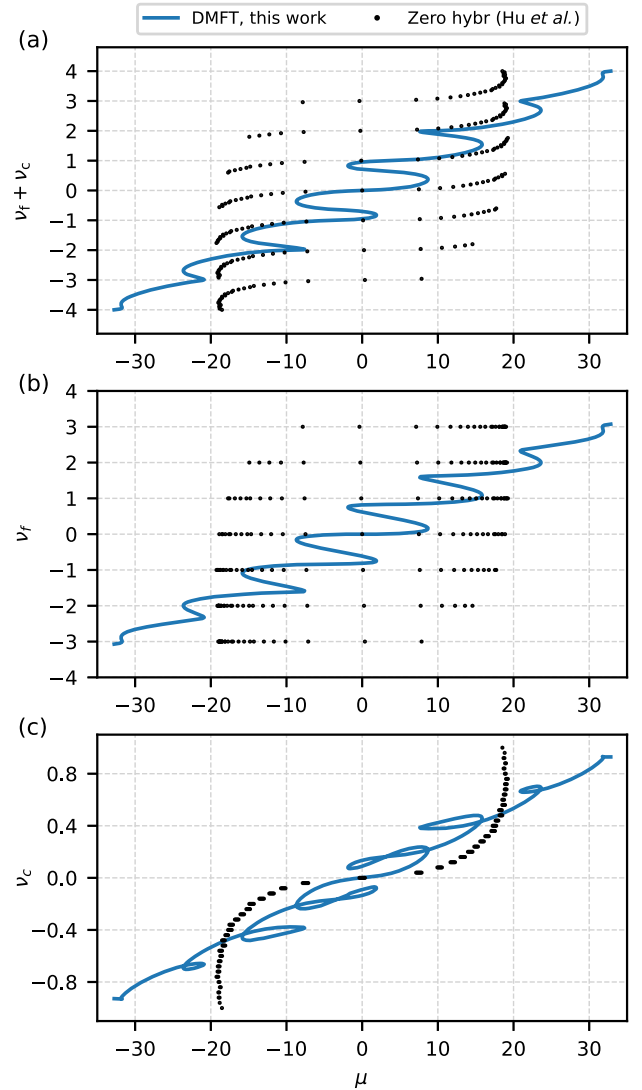


FIG. 6. Filling with respect to CNP as a function of the chemical potential. (a) Total filling, (b) f -electron filling, and (c) c -electron filling at $T = 11.6$ K. The solid blue curves refer to DMFT simulations tuning the chemical potential to obtain a target (total) filling. The black dots show results for the zero-hybridization model solved in Ref. [200].

accounted for in our charge self-consistent DMFT calculation can be found in the Supplemental Material [204] (see also Refs. [226–228] therein); in short, this amounts to separating intrinsic from geometric contributions to the thermodynamic potential [229,230] and to the chemical potential. What follows uses the intrinsic chemical potential μ unless otherwise stated.

The blue solid lines in Fig. 6 report the total and orbital-resolved fillings as a function of μ . These are to be compared with the black dots, which report the same for the zero-hybridization model. In both cases, the overall behavior of the filling is a consequence of an energetic balance between the orbital species. The f - c hybridization

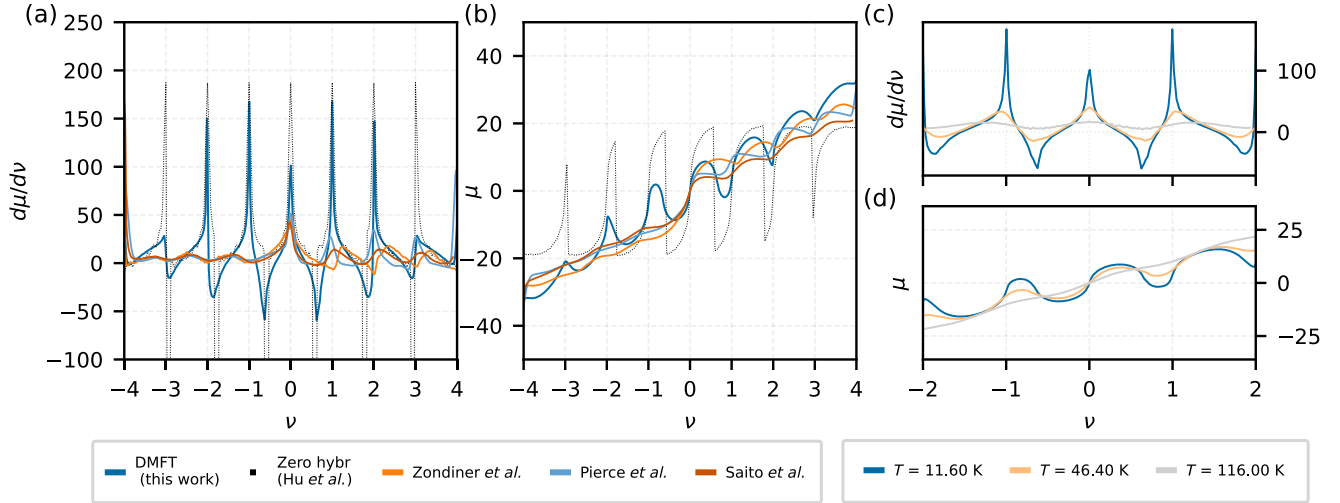


FIG. 7. (a) Inverse compressibility obtained from the fixed-occupation DMFT simulations for $T = 11.6$ K, compared with the experimental data from Zondiner *et al.* [194] ($B_{\parallel} = 0$, $T = 4$ K, and $\theta = 1.13^{\circ}$), Pierce *et al.* [191] ($B_{\parallel} = 0$, $\theta = 1.06^{\circ}$), and Saito *et al.* [164] ($B_{\parallel} = 0$, $T = 12$ K, and $\theta = 1.06^{\circ}$), and the zero-hybridization model from Ref. [200]. (b) The chemical potential corresponding to the inverse compressibilities in (a). (c) Inverse compressibility and (d) chemical potential as a function of doping for three different temperatures.

constitutes the additional feature captured by our DMFT study with respect to the zero-hybridization case described in Ref. [200], and causes a breakdown of the rigid-band picture. The role of the f - c hybridization is to provide a “smoothing” effect on the crosstalk between the two subspaces. Note that, differently from the standard periodic Anderson models considered in literature, the THF model [17] features a specific momentum, and hence real-space, dependence of the hybridization term $H^{fc}(\mathbf{k})$.

The capricious ups and downs of ν_c shown in Fig. 6(c) have to be contrasted to the progressive filling of the uncoupled reservoir of itinerant electrons in the zero-hybridization case: In both cases, when an additional flat f -electron band passes through the Fermi level, it provides a large, rapid increase in occupation, which is compensated by emptying the dispersive c bands. This behavior is discontinuous in the decoupled case, with ν_c traveling multiple times from ≈ -0.85 to $\approx +0.85$ along the same path marked by the black dots in Fig. 6(c). By contrast, the presence of f - c hybridization and broadening in the DMFT solution forces both ν_f and ν_c to vary continuously. This results in the behaviors highlighted by the blue curves in Figs. 6(b) and 6(c), respectively: The f -electron occupation monotonically increases with respect to the total ν [see also Fig. 5(a)]; when pictured upon varying μ , it shows a series of continuously connected plateaus. These occur trivially at integer values in the zero-hybridization model, while the DMFT solution with hybridization displays plateaus that are not pinned to integer ν_f , except obviously for $\nu_f = 0$ because of particle-hole symmetry. Because of the previously mentioned occupation balancing mechanism, ν_c has instead to necessarily decrease in some intervals upon

increasing the total ν , resulting in the peculiar “loops” of Fig. 6(c). A movie showing the evolution of the momentum-resolved spectral function across the filling range is included in the Supplemental Material [204]. It clearly shows the mutual transfer of low-energy spectral weight between f and c .

For comparison to experiments, we extract the electronic compressibility of the model and plot its inverse in Fig. 7(a). One can see how the full resets of μ in the zero-hybridization case result in extremely pronounced negative spikes. In DMFT, these negative regions are much less prominent and their intensity varies with doping with respect to the charge neutrality point. However, the minima of the DMFT data coincide with the negative spikes of the zero-hybridization model, and the positive spikes at integer fillings are consistent between the two methods. While the maxima in the compressibilities found here and by the DMFT study of Datta *et al.* [186] are in qualitative agreement, there are no negative compressibilities reported in Ref. [186]. We assign this discrepancy to geometric capacitance terms, which may not have been fully subtracted in Ref. [186].

The comparison of our DMFT results to experiments, shown in Figs. 7(a) and 7(b), reveals an overall reasonable agreement between DMFT and experiments from Refs. [164,191,194]. Yet, even if DMFT suppresses the negative compressibilities with respect to zero hybridization, it still overestimates the regions of negative compressibility compared to what is experimentally observed [compare the dark blue curve to the others in Fig. 7(a)]. Among the different experimental curves, showing some discrepancies between one another, it is interesting to notice how the position of the DMFT positive peaks at integer fillings match rather well those of Ref. [191], while the

negative peaks and the overall behavior of the chemical potential are more similar to that of Ref. [194]. Since the THF model is by design particle-hole symmetric, it does not account for the asymmetries experimentally measured for electron and hole doping. Our results are a better match for positive doping than negative doping. A calculation including strain and additional particle-hole symmetry breaking terms will be the subject of a future study.

In Figs. 7(c) and 7(d), we show the temperature dependence of the inverse compressibility and the chemical potential. The peaks in the inverse compressibility (step features in the chemical potential) get progressively thermally broadened and are almost completely washed out at ~ 100 K. This compares nicely with experimental reports on the temperature dependence of the inverse compressibility [164], where the features also wash out at ~ 100 K. This is the temperature scale at which thermally activated charge fluctuations become appreciable and the Hartree-Fock solution is no longer isospin polarized. In the Supplemental Material [204], we confirm by calculating the temperature-dependent sector statistics (the weight of the different charge sectors in the many-body configurations) that this is also the temperature scale where there is no longer one predominant charge sector. In other words, the experimentally observed structures of the inverse compressibility and its temperature dependence pinpoint the thermal activation of charge fluctuations and the dissolution of local moment physics around ~ 100 K.

I. Significance and origin of the negative compressibilities

All chemical potential terms discussed so far referred to the intrinsic chemical potential, while only the total thermodynamic potential determines instabilities of the system. The total thermodynamic potential has to include also the geometric contributions, which are present in both, the theoretical model [17], and all experimental realizations of TBLG [156,163,164,194]: The charge required to dope TBLG away from charge neutrality is taken from gate electrodes. The geometric contribution to the total thermodynamic potential is the classical electrostatic energy that builds up upon charge transfer from the gate to TBLG. The intrinsic chemical potential does not involve the contribution from electrostatic potential associated with the charge transfer between gate and TBLG and thus, in turn, a negative compressibility referring only to a derivative involving the intrinsic chemical potential $dn/d\mu$ does neither imply necessarily an instability of the system nor a tendency to phase separate.

In the THF model of Ref. [17], the TBLG system is supposed to sit in the middle of two gate electrodes, providing an electric potential dependent on the gate separation. As detailed in the Supplemental Material [204], this entails a large geometric capacitance term, which has to be taken into account when determining the *total* TBLG

compressibility. In the Supplemental Material [204], we show the same data of Figs. 6 and 7, plotted without the subtraction of the geometrical capacitance contribution, i.e., referring to the *full* TBLG system, which necessarily includes the gates where the doping charges are taken from. There, most of the negative compressibility regions are gone, though a small region survives close to $\nu \pm 0.6$. As detailed in the Supplemental Material [204], this effect is related to the form of the double-gate screened Coulomb integrals considered in the original THF model, which sets an intergate distance $\xi = 10$ nm [17]. The geometric contribution depends linearly on the distance between the capacitor plates, which suggests that an interaction term corresponding to a larger separation would have removed even the remaining $\nu \pm 0.6$ negative compressibility region. Similar geometric effects are also ubiquitously present in experimental realizations [156,163,164,194], where TBLG is typically placed in single or multigate structures in order to achieve gate controlled charge doping. In the experimentally realized setups, assuming the electrodes or backgate to be ideal metals, which do not feature quantum capacitance effects, the only contribution to the negative compressibility comes from exchange-correlation contributions on the TBLG layer [231], which are accounted for in DMFT locally to all orders.

V. CONCLUSIONS

Our study provides a unified understanding of dynamic correlations and spontaneous symmetry breaking in TBLG, allowing us to reconcile a set of complementary experiments spanning a wide range of temperatures. Strong electronic interactions give rise to the emergence of local isospin moments at temperatures on the order of ~ 100 K, which order around ~ 10 K. This result suggests that ordering precedes full Kondo screening which manifests at lower temperatures [188]. Furthermore, our comparison between DMFT and Hartree-Fock ordering temperatures reveals a noteworthy difference of one order of magnitude, indicating the significant influence of local quantum fluctuations on the temperature-dependent phase diagram of TBLG. Note that the true ordering temperatures will be lower than what is predicted by single-site DMFT, as it neglects spatial fluctuations.

Once the local moments have formed, regardless of whether they order or not, exchange-correlation effects in the localized f states lead to “integerperiodic” variations in the compressibility ranging from nearly incompressible to negative values as found in capacitance experiments [164,191,194]. Concomitantly, there is a periodic redistribution of charge between the f and the c states upon doping. This charge reshuffling is responsible for the doping-induced cascade transitions seen in scanning tunneling spectroscopy [156] and explains why the cascades first appear at a temperature of ~ 100 K [164].

Our study focuses on finite temperatures $T \gtrsim 5$ K and highlights the special role of total integer fillings and the

appearance of (nearly) incompressible insulating states there. While there is a depletion of low-energy spectral weight already in the symmetric phase, exchange interactions generically support a hard gap at integer fillings in the ordered phase in the absence of strain.

Regarding the nature of the metallic states in TBLG, we find disordered local moments which cause scattering and predominantly incoherent low-energy electronic spectral weight in the temperature range of approximately $10 < T < 100$ K. Ordering of the isospin moments leads to coherence and the appearance of well-defined quasiparticles for $T \lesssim 10$ K. This order-induced coherence stands behind the isospin Pomeranchuk effect observed in transport experiments. Above the ordering temperature but below the temperature of moment formation, the isospin entropy of the local moments stabilizes an incoherent “bad metal” phase, which manifests in incoherent spectral weight at the Fermi level. Below the ordering temperature, the Fermi surface is composed of delocalized coherent quasiparticle excitations implying Fermi-liquid-like behavior. This change from incoherent to coherent spectral weight at the Fermi level can explain the generic resistivity drop seen in many experiments below ~ 10 K [6,151,161,163,164]. In contrast to the original Pomeranchuk effect in He-3, the suppression of entropy and coherence in TBLG at low temperatures come from the ordering of local moments and not from their disappearance. The coherence from order physics demonstrated here for TLBG reveals similarities between TBLG and materials such as metallic ferromagnets like SrRuO₃ [223] and compounds related to Fe-based superconductors [224].

We note that the single-site DMFT neglects nonlocal fluctuations and any dynamical renormalization effects on \hat{H}_J . Both of these approximations will lead to an overestimate of the ordering temperature, so the true ordering temperature is likely to be a bit lower. The renormalization of \hat{H}_J is expected to be weak except possibly far away from integer fillings, which is also where the filling-dependent Kondo temperature is expected to find its local maxima (see Ref. [189] and Supplemental Material [204]). These effects, however, are likely secondary to strain and particle-hole symmetry breaking lattice effects [232], which have been shown to have a huge effect on the low-temperature ordered states [61,64,108,109]. The inclusion of these effects is a natural extension of our work.

Our results show that ordering affects electronic spectra and even Fermi surface topologies in metallic states. Thus, we expect that further symmetry breaking, i.e., particularly superconductivity at lower temperatures $T \sim 1$ K, will be impacted by this order-facilitated coherence.

ACKNOWLEDGMENTS

We thank Dimitri Efetov, Piers Coleman, Andrew Millis, Alexei M. Tsvelik, Sankar Das Sarma, Xi Dai, Andrey Chubukov, Francisco Guinea, Maria J. Calderón, Leni Bascones, Ali Yazdani, Shahal Ilani, Pablo Jarillo-Herrero,

Silke Paschen, Elio König, Philipp Eck, and Georg Rohringer for useful discussions. G. R. and T. W. gratefully acknowledge funding and support from the European Commission via the Graphene Flagship Core Project 3 (Grant Agreement No. 881603), the Deutsche Forschungsgemeinschaft (DFG, German Research Foundation) through the cluster of excellence “CUI: Advanced Imaging of Matter” of the Deutsche Forschungsgemeinschaft (DFG EXC 2056, Project No. 390715994), and the DFG priority program SPP2244 (Project No. 443274199). G. R., L. C., T. W., G. S., and R. V. thank the DFG for funding through the research unit QUAFT FOR 5249 (Project No. 449872909; Projects P4 and P5). G. R. gratefully acknowledges the computing time granted by the Resource Allocation Board and provided on the supercomputer Lise and Emmy at NHR@ZIB and NHR@Göttingen as part of the NHR infrastructure (Project No. hhp00061). L. C. and G. S. were supported by the Würzburg-Dresden Cluster of Excellence on Complexity and Topology in Quantum Matter—ct.qmat Project No. 390858490-EXC 2147, and gratefully acknowledge the Gauss Centre for Supercomputing e.V. for funding this project by providing computing time on the GCS Supercomputer SuperMUC at Leibniz Supercomputing Centre. L. C. gratefully acknowledges the scientific support and HPC resources provided by the Erlangen National High Performance Computing Center (NHR@FAU) of the Friedrich-Alexander-Universität Erlangen-Nürnberg (FAU) under the NHR Project No. b158cb. NHR funding is provided by federal and Bavarian state authorities. NHR@FAU hardware is partially funded by the German Research Foundation (DFG)—440719683. The research of R. V. was supported in part by the National Science Foundation under Grants No. NSF PHY-1748958 and No. PHY-2309135. L. d. M. is supported by the European Commission through the ERC-CoG2016, StrongCoPhy4Energy, Grant Agreement No. 724177. The work of B. A. B. was primarily supported by the DOE Grant No. DE-SC0016239, the Simons Investigator Grant No. 404513. H. H. was supported by the European Research Council (ERC) under the European Union’s Horizon 2020 research and innovation program (Grant Agreement No. 101020833). D. C. was supported by the DOE Grant No. DE-SC0016239 by the Gordon and Betty Moore Foundation through Grant No. GBMF8685 toward the Princeton theory program, the Gordon and Betty Moore Foundation’s EPiQS Initiative (Grant No. GBMF11070), Office of Naval Research (ONR Grant No. N00014-20-1-2303), BSF Israel U.S. foundation No. 2018226 and NSF-MERSEC DMR. The Flatiron Institute is a division of the Simons Foundation.

-
- [1] E. Suárez Morell, J. D. Correa, P. Vargas, M. Pacheco, and Z. Barticevic, *Flat bands in slightly twisted bilayer graphene: Tight-binding calculations*, *Phys. Rev. B* **82**, 121407(R) (2010).

- [2] J. M. B. Lopes dos Santos, N. M. R. Peres, and A. H. Castro Neto, *Graphene bilayer with a twist: Electronic structure*, *Phys. Rev. Lett.* **99**, 256802 (2007).
- [3] R. Bistritzer and A. H. MacDonald, *Moiré bands in twisted double-layer graphene*, *Proc. Natl. Acad. Sci. U.S.A.* **108**, 12233 (2011).
- [4] Y. Ren, Q. Gao, A. H. MacDonald, and Q. Niu, *WKB estimate of bilayer graphene's magic twist angles*, *Phys. Rev. Lett.* **126**, 016404 (2021).
- [5] Y. Cao, V. Fatemi, S. Fang, K. Watanabe, T. Taniguchi, E. Kaxiras, and P. Jarillo-Herrero, *Unconventional superconductivity in magic-angle graphene superlattices*, *Nature (London)* **556**, 43 (2018).
- [6] X. Lu, P. Stepanov, W. Yang, M. Xie, M. A. Aamir, I. Das, C. Urgell, K. Watanabe, T. Taniguchi, G. Zhang, A. Bachtold, A. H. MacDonald, and D. K. Efetov, *Superconductors, orbital magnets and correlated states in magic-angle bilayer graphene*, *Nature (London)* **574**, 653 (2019).
- [7] M. Oh, K. P. Nuckolls, D. Wong, R. L. Lee, X. Liu, K. Watanabe, T. Taniguchi, and A. Yazdani, *Evidence for unconventional superconductivity in twisted bilayer graphene*, *Nature (London)* **600**, 240 (2021).
- [8] M. Yankowitz, S. Chen, H. Polshyn, Y. Zhang, K. Watanabe, T. Taniguchi, D. Graf, A. F. Young, and C. R. Dean, *Tuning superconductivity in twisted bilayer graphene*, *Science* **363**, 1059 (2019).
- [9] Y. Cao, V. Fatemi, A. Demir, S. Fang, S. L. Tomarken, J. Y. Luo, J. D. Sanchez-Yamagishi, K. Watanabe, T. Taniguchi, E. Kaxiras, R. C. Ashoori, and P. Jarillo-Herrero, *Correlated insulator behaviour at half-filling in magic-angle graphene superlattices*, *Nature (London)* **556**, 80 (2018).
- [10] H. Polshyn, M. Yankowitz, S. Chen, Y. Zhang, K. Watanabe, T. Taniguchi, C. R. Dean, and A. F. Young, *Large linear-in-temperature resistivity in twisted bilayer graphene*, *Nat. Phys.* **15**, 1011 (2019).
- [11] A. Jaoui, I. Das, G. Di Battista, J. Díez-Mérida, X. Lu, K. Watanabe, T. Taniguchi, H. Ishizuka, L. Levitov, and D. K. Efetov, *Quantum critical behaviour in magic-angle twisted bilayer graphene*, *Nat. Phys.* **18**, 633 (2022).
- [12] K. P. Nuckolls, M. Oh, D. Wong, B. Lian, K. Watanabe, T. Taniguchi, B. A. Bernevig, and A. Yazdani, *Strongly correlated Chern insulators in magic-angle twisted bilayer graphene*, *Nature (London)* **588**, 610 (2020).
- [13] M. Serlin, C. L. Tschirhart, H. Polshyn, Y. Zhang, J. Zhu, K. Watanabe, T. Taniguchi, L. Balents, and A. F. Young, *Intrinsic quantized anomalous Hall effect in a moiré heterostructure*, *Science* **367**, 900 (2020).
- [14] A. L. Sharpe, E. J. Fox, A. W. Barnard, J. Finney, K. Watanabe, T. Taniguchi, M. A. Kastner, and D. Goldhaber-Gordon, *Emergent ferromagnetism near three-quarters filling in twisted bilayer graphene*, *Science* **365**, 605 (2019).
- [15] Y. Xie, A. T. Pierce, J. M. Park, D. E. Parker, E. Khalaf, P. Ledwith, Y. Cao, S. H. Lee, S. Chen, P. R. Forrester, K. Watanabe, T. Taniguchi, A. Vishwanath, P. Jarillo-Herrero, and A. Yacoby, *Fractional Chern insulators in magic-angle twisted bilayer graphene*, *Nature (London)* **600**, 439 (2021).
- [16] G. Chen, A. L. Sharpe, E. J. Fox, Y.-H. Zhang, S. Wang, L. Jiang, B. Lyu, H. Li, K. Watanabe, T. Taniguchi, Z. Shi, T. Senthil, D. Goldhaber-Gordon, Y. Zhang, and F. Wang, *Tunable correlated Chern insulator and ferromagnetism in a moiré superlattice*, *Nature (London)* **579**, 56 (2020).
- [17] Z.-D. Song and B. A. Bernevig, *Magic-angle twisted bilayer graphene as a topological heavy fermion problem*, *Phys. Rev. Lett.* **129**, 047601 (2022).
- [18] D. M. Kennes, J. Lischner, and C. Karrasch, *Strong correlations and $d + id$ superconductivity in twisted bilayer graphene*, *Phys. Rev. B* **98**, 241407(R) (2018).
- [19] X.-C. Wu, C.-M. Jian, and C. Xu, *Coupled-wire description of the correlated physics in twisted bilayer graphene*, *Phys. Rev. B* **99**, 161405(R) (2019).
- [20] T. Huang, L. Zhang, and T. Ma, *Antiferromagnetically ordered Mott insulator and $d + id$ superconductivity in twisted bilayer graphene: A quantum Monte Carlo study*, *Sci. Bull.* **64**, 310 (2019).
- [21] L. Classen, C. Honerkamp, and M. M. Scherer, *Competing phases of interacting electrons on triangular lattices in moiré heterostructures*, *Phys. Rev. B* **99**, 195120 (2019).
- [22] M. Christos, S. Sachdev, and M. S. Scheurer, *Superconductivity, correlated insulators, and Wess-Zumino-Witten terms in twisted bilayer graphene*, *Proc. Natl. Acad. Sci. U.S.A.* **117**, 29543 (2020).
- [23] Y. Saito, J. Ge, K. Watanabe, T. Taniguchi, and A. F. Young, *Independent superconductors and correlated insulators in twisted bilayer graphene*, *Nat. Phys.* **16**, 926 (2020).
- [24] A. Thomson, S. Chatterjee, S. Sachdev, and M. S. Scheurer, *Triangular antiferromagnetism on the honeycomb lattice of twisted bilayer graphene*, *Phys. Rev. B* **98**, 075109 (2018).
- [25] L. Rademaker and P. Mellado, *Charge-transfer insulation in twisted bilayer graphene*, *Phys. Rev. B* **98**, 235158 (2018).
- [26] M. Ochi, M. Koshino, and K. Kuroki, *Possible correlated insulating states in magic-angle twisted bilayer graphene under strongly competing interactions*, *Phys. Rev. B* **98**, 081102(R) (2018).
- [27] B. Padhi, C. Setty, and P. W. Phillips, *Doped twisted bilayer graphene near magic angles: Proximity to Wigner crystallization, not Mott insulation*, *Nano Lett.* **18**, 6175 (2018).
- [28] X. Y. Xu, K. T. Law, and P. A. Lee, *Kekulé valence bond order in an extended Hubbard model on the honeycomb lattice with possible applications to twisted bilayer graphene*, *Phys. Rev. B* **98**, 121406(R) (2018).
- [29] J. Liu, J. Liu, and X. Dai, *Pseudo Landau level representation of twisted bilayer graphene: Band topology and implications on the correlated insulating phase*, *Phys. Rev. B* **99**, 155415 (2019).
- [30] L. Rademaker, D. A. Abanin, and P. Mellado, *Charge smoothening and band flattening due to Hartree corrections in twisted bilayer graphene*, *Phys. Rev. B* **100**, 205114 (2019).
- [31] J. Kang and O. Vafek, *Strong coupling phases of partially filled twisted bilayer graphene narrow bands*, *Phys. Rev. Lett.* **122**, 246401 (2019).

- [32] T. Cea and F. Guinea, *Band structure and insulating states driven by Coulomb interaction in twisted bilayer graphene*, *Phys. Rev. B* **102**, 045107 (2020).
- [33] E. Khalaf, N. Bultinck, A. Vishwanath, and M. P. Zaletel, *Soft modes in magic angle twisted bilayer graphene*, arXiv:2009.14827.
- [34] O. Vafek and J. Kang, *Renormalization group study of hidden symmetry in twisted bilayer graphene with Coulomb interactions*, *Phys. Rev. Lett.* **125**, 257602 (2020).
- [35] P. Eugenio and C. Dag, *DMRG study of strongly interacting \mathbb{Z}_2 flatbands: A toy model inspired by twisted bilayer graphene*, *SciPost Phys. Core* **3**, 015 (2020).
- [36] Y. Zhang, K. Jiang, Z. Wang, and F. Zhang, *Correlated insulating phases of twisted bilayer graphene at commensurate filling fractions: A Hartree-Fock study*, *Phys. Rev. B* **102**, 035136 (2020).
- [37] T. Soejima, D. E. Parker, N. Bultinck, J. Hauschild, and M. P. Zaletel, *Efficient simulation of moiré materials using the density matrix renormalization group*, *Phys. Rev. B* **102**, 205111 (2020).
- [38] N. Bultinck, E. Khalaf, S. Liu, S. Chatterjee, A. Vishwanath, and M. P. Zaletel, *Ground state and hidden symmetry of magic-angle graphene at even integer filling*, *Phys. Rev. X* **10**, 031034 (2020).
- [39] M. Xie and A. H. MacDonald, *Nature of the correlated insulator states in twisted bilayer graphene*, *Phys. Rev. Lett.* **124**, 097601 (2020).
- [40] E. Brillaux, D. Carpentier, A. A. Fedorenko, and L. Savary, *Analytical renormalization group approach to competing orders at charge neutrality in twisted bilayer graphene*, *Phys. Rev. Res.* **4**, 033168 (2022).
- [41] J. Kang and O. Vafek, *Non-Abelian Dirac node braiding and near-degeneracy of correlated phases at odd integer filling in magic-angle twisted bilayer graphene*, *Phys. Rev. B* **102**, 035161 (2020).
- [42] S. Chatterjee, N. Bultinck, and M. P. Zaletel, *Symmetry breaking and skyrmionic transport in twisted bilayer graphene*, *Phys. Rev. B* **101**, 165141 (2020).
- [43] P. J. Ledwith, G. Tarnopolsky, E. Khalaf, and A. Vishwanath, *Fractional Chern insulator states in twisted bilayer graphene: An analytical approach*, *Phys. Rev. Res.* **2**, 023237 (2020).
- [44] D. V. Chichinadze, L. Classen, and A. V. Chubukov, *Valley magnetism, nematicity, and density wave orders in twisted bilayer graphene*, *Phys. Rev. B* **102**, 125120 (2020).
- [45] A. Abouelkomsan, Z. Liu, and E. J. Bergholtz, *Particle-hole duality, emergent Fermi liquids, and fractional Chern insulators in moiré flatbands*, *Phys. Rev. Lett.* **124**, 106803 (2020).
- [46] C. Repellin and T. Senthil, *Chern bands of twisted bilayer graphene: Fractional Chern insulators and spin phase transition*, *Phys. Rev. Res.* **2**, 023238 (2020).
- [47] S. Xu, M. M. Al Ezzi, N. Balakrishnan, A. Garcia-Ruiz, B. Tsim, C. Mullan, J. Barrier, N. Xin, B. A. Piot, T. Taniguchi, K. Watanabe, A. Carvalho, A. Mishchenko, A. K. Geim, V. I. Fal'ko, S. Adam, A. H. C. Neto, K. S. Novoselov, and Y. Shi, *Tunable van Hove singularities and correlated states in twisted monolayer-bilayer graphene*, *Nat. Phys.* **17**, 619 (2021).
- [48] D. E. Parker, T. Soejima, J. Hauschild, M. P. Zaletel, and N. Bultinck, *Strain-induced quantum phase transitions in magic-angle graphene*, *Phys. Rev. Lett.* **127**, 027601 (2021).
- [49] Y. H. Kwan, G. Wagner, N. Chakraborty, S. H. Simon, and S. A. Parameswaran, *Domain wall competition in the Chern insulating regime of twisted bilayer graphene*, *Phys. Rev. B* **104**, 115404 (2021).
- [50] Y. H. Kwan, Y. Hu, S. H. Simon, and S. A. Parameswaran, *Exciton band topology in spontaneous quantum anomalous Hall insulators: Applications to twisted bilayer graphene*, *Phys. Rev. Lett.* **126**, 137601 (2021).
- [51] B.-B. Chen, Y. D. Liao, Z. Chen, O. Vafek, J. Kang, W. Li, and Z. Y. Meng, *Realization of topological Mott insulator in a twisted bilayer graphene lattice model*, *Nat. Commun.* **12**, 5480 (2021).
- [52] X. Zhang, G. Pan, Y. Zhang, J. Kang, and Z. Y. Meng, *Momentum space quantum Monte Carlo on twisted bilayer graphene*, *Chin. Phys. Lett.* **38**, 077305 (2021).
- [53] J. Kang, B. A. Bernevig, and O. Vafek, *Cascades between light and heavy fermions in the normal state of magic-angle twisted bilayer graphene*, *Phys. Rev. Lett.* **127**, 266402 (2021).
- [54] A. Kumar, M. Xie, and A. H. MacDonald, *Lattice collective modes from a continuum model of magic-angle twisted bilayer graphene*, *Phys. Rev. B* **104**, 035119 (2021).
- [55] Y. D. Liao, J. Kang, C. N. Breið, X. Y. Xu, H.-Q. Wu, B. M. Andersen, R. M. Fernandes, and Z. Y. Meng, *Correlation-induced insulating topological phases at charge neutrality in twisted bilayer graphene*, *Phys. Rev. X* **11**, 011014 (2021).
- [56] S. Wu, Z. Zhang, K. Watanabe, T. Taniguchi, and E. Y. Andrei, *Chern insulators, van Hove singularities and topological flat bands in magic-angle twisted bilayer graphene*, *Nat. Mater.* **20**, 488 (2021).
- [57] B. Lian, Z.-D. Song, N. Regnault, D. K. Efetov, A. Yazdani, and B. A. Bernevig, *Twisted bilayer graphene. IV. Exact insulator ground states and phase diagram*, *Phys. Rev. B* **103**, 205414 (2021).
- [58] J. Liu and X. Dai, *Theories for the correlated insulating states and quantum anomalous Hall effect phenomena in twisted bilayer graphene*, *Phys. Rev. B* **103**, 035427 (2021).
- [59] F. Xie, A. Cowsik, Z.-D. Song, B. Lian, B. A. Bernevig, and N. Regnault, *Twisted bilayer graphene. VI. An exact diagonalization study at nonzero integer filling*, *Phys. Rev. B* **103**, 205416 (2021).
- [60] S. Liu, E. Khalaf, J. Y. Lee, and A. Vishwanath, *Nematic topological semimetal and insulator in magic-angle bilayer graphene at charge neutrality*, *Phys. Rev. Res.* **3**, 013033 (2021).
- [61] Y. H. Kwan, G. Wagner, T. Soejima, M. P. Zaletel, S. H. Simon, S. A. Parameswaran, and N. Bultinck, *Kekulé spiral order at all nonzero integer fillings in twisted bilayer graphene*, *Phys. Rev. X* **11**, 041063 (2021).
- [62] J. S. Hofmann, E. Khalaf, A. Vishwanath, E. Berg, and J. Y. Lee, *Fermionic Monte Carlo study of a realistic model of twisted bilayer graphene*, *Phys. Rev. X* **12**, 011061 (2022).

- [63] F. Xie, J. Kang, B. A. Bernevig, O. Vafek, and N. Regnault, *Phase diagram of twisted bilayer graphene at filling factor $\nu = \pm 3$* , *Phys. Rev. B* **107**, 075156 (2023).
- [64] G. Wagner, Y. H. Kwan, N. Bultinck, S. H. Simon, and S. A. Parameswaran, *Global phase diagram of the normal state of twisted bilayer graphene*, *Phys. Rev. Lett.* **128**, 156401 (2022).
- [65] X. Zhang, G. Pan, B.-B. Chen, H. Li, K. Sun, and Z. Y. Meng, *Polynomial sign problem and topological Mott insulator in twisted bilayer graphene*, *Phys. Rev. B* **107**, L241105 (2023).
- [66] M. Christos, S. Sachdev, and M. S. Scheurer, *Correlated insulators, semimetals, and superconductivity in twisted trilayer graphene*, *Phys. Rev. X* **12**, 021018 (2022).
- [67] Y. Da Liao, Z. Y. Meng, and X. Y. Xu, *Valence bond orders at charge neutrality in a possible two-orbital extended Hubbard model for twisted bilayer graphene*, *Phys. Rev. Lett.* **123**, 157601 (2019).
- [68] P. Cha, A. A. Patel, and E.-A. Kim, *Strange metals from melting correlated insulators in twisted bilayer graphene*, *Phys. Rev. Lett.* **127**, 266601 (2021).
- [69] Y. Sheffer and A. Stern, *Chiral magic-angle twisted bilayer graphene in a magnetic field: Landau level correspondence, exact wave functions, and fractional Chern insulators*, *Phys. Rev. B* **104**, L121405 (2021).
- [70] P. Potasz, M. Xie, and A. H. MacDonald, *Exact diagonalization for magic-angle twisted bilayer graphene*, *Phys. Rev. Lett.* **127**, 147203 (2021).
- [71] D. Călugăru, N. Regnault, M. Oh, K. P. Nuckolls, D. Wong, R. L. Lee, A. Yazdani, O. Vafek, and B. A. Bernevig, *Spectroscopy of twisted bilayer graphene correlated insulators*, *Phys. Rev. Lett.* **129**, 117602 (2022).
- [72] F. Wu and S. Das Sarma, *Collective excitations of quantum anomalous Hall ferromagnets in twisted bilayer graphene*, *Phys. Rev. Lett.* **124**, 046403 (2020).
- [73] K. Seo, V. N. Kotov, and B. Uchoa, *Ferromagnetic Mott state in twisted graphene bilayers at the magic angle*, *Phys. Rev. Lett.* **122**, 246402 (2019).
- [74] C. Repellin, Z. Dong, Y.-H. Zhang, and T. Senthil, *Ferromagnetism in narrow bands of moiré superlattices*, *Phys. Rev. Lett.* **124**, 187601 (2020).
- [75] N. Bultinck, S. Chatterjee, and M. P. Zaletel, *Mechanism for anomalous Hall ferromagnetism in twisted bilayer graphene*, *Phys. Rev. Lett.* **124**, 166601 (2020).
- [76] J. Herzog-Arbeitman, A. Chew, D. K. Efetov, and B. A. Bernevig, *Reentrant correlated insulators in twisted bilayer graphene at 25 T (2π flux)*, *Phys. Rev. Lett.* **129**, 076401 (2022).
- [77] C. Huang, X. Zhang, G. Pan, H. Li, K. Sun, X. Dai, and Z. Y. Meng, *Evolution from quantum anomalous Hall insulator to heavy-fermion semimetal in magic-angle twisted bilayer graphene*, *Phys. Rev. B* **109**, 125404 (2024).
- [78] Z. Liu, E. J. Bergholtz, H. Fan, and A. M. Läuchli, *Fractional Chern insulators in topological flat bands with higher Chern number*, *Phys. Rev. Lett.* **109**, 186805 (2012).
- [79] F. Guinea and N. R. Walet, *Electrostatic effects, band distortions, and superconductivity in twisted graphene bilayers*, *Proc. Natl. Acad. Sci. U.S.A.* **115**, 13174 (2018).
- [80] F. Wu, A. H. MacDonald, and I. Martin, *Theory of phonon-mediated superconductivity in twisted bilayer graphene*, *Phys. Rev. Lett.* **121**, 257001 (2018).
- [81] H. Guo, X. Zhu, S. Feng, and R. T. Scalettar, *Pairing symmetry of interacting fermions on a twisted bilayer graphene superlattice*, *Phys. Rev. B* **97**, 235453 (2018).
- [82] C.-C. Liu, L.-D. Zhang, W.-Q. Chen, and F. Yang, *Chiral spin density wave and $d + id$ superconductivity in the magic-angle-twisted bilayer graphene*, *Phys. Rev. Lett.* **121**, 217001 (2018).
- [83] T. J. Peltonen, R. Ojajärvi, and T. T. Heikkilä, *Mean-field theory for superconductivity in twisted bilayer graphene*, *Phys. Rev. B* **98**, 220504(R) (2018).
- [84] C. Xu and L. Balents, *Topological superconductivity in twisted multilayer graphene*, *Phys. Rev. Lett.* **121**, 087001 (2018).
- [85] H. Isobe, N. F. Q. Yuan, and L. Fu, *Unconventional superconductivity and density waves in twisted bilayer graphene*, *Phys. Rev. X* **8**, 041041 (2018).
- [86] Y.-Z. You and A. Vishwanath, *Superconductivity from valley fluctuations and approximate SO(4) symmetry in a weak coupling theory of twisted bilayer graphene*, *npj Quantum Mater.* **4**, 1 (2019).
- [87] B. Lian, Z. Wang, and B. A. Bernevig, *Twisted bilayer graphene: A phonon-driven superconductor*, *Phys. Rev. Lett.* **122**, 257002 (2019).
- [88] J. González and T. Stauber, *Kohn-Luttinger superconductivity in twisted bilayer graphene*, *Phys. Rev. Lett.* **122**, 026801 (2019).
- [89] B. Roy and V. Juričić, *Unconventional superconductivity in nearly flat bands in twisted bilayer graphene*, *Phys. Rev. B* **99**, 121407(R) (2019).
- [90] A. Julku, T. J. Peltonen, L. Liang, T. T. Heikkilä, and P. Törmä, *Superfluid weight and Berezinskii-Kosterlitz-Thouless transition temperature of twisted bilayer graphene*, *Phys. Rev. B* **101**, 060505(R) (2020).
- [91] E. J. König, P. Coleman, and A. M. Tsvelik, *Spin magnetometry as a probe of stripe superconductivity in twisted bilayer graphene*, *Phys. Rev. B* **102**, 104514 (2020).
- [92] S. Chatterjee, M. Ippoliti, and M. P. Zaletel, *Skymion superconductivity: DMRG evidence for a topological route to superconductivity*, *Phys. Rev. B* **106**, 035421 (2022).
- [93] D. V. Chichinadze, L. Classen, and A. V. Chubukov, *Nematic superconductivity in twisted bilayer graphene*, *Phys. Rev. B* **101**, 224513 (2020).
- [94] E. Khalaf, S. Chatterjee, N. Bultinck, M. P. Zaletel, and A. Vishwanath, *Charged skyrmions and topological origin of superconductivity in magic-angle graphene*, *Sci. Adv.* **7**, eabf5299 (2021).
- [95] C. Lewandowski, D. Chowdhury, and J. Ruhman, *Pairing in magic-angle twisted bilayer graphene: Role of phonon and plasmon umklapp*, *Phys. Rev. B* **103**, 235401 (2021).
- [96] Y. Wang, J. Kang, and R. M. Fernandes, *Topological and nematic superconductivity mediated by ferro-SU(4) fluctuations in twisted bilayer graphene*, *Phys. Rev. B* **103**, 024506 (2021).
- [97] J. M. Park, Y. Cao, K. Watanabe, T. Taniguchi, and P. Jarillo-Herrero, *Tunable strongly coupled superconductivity in magic-angle twisted trilayer graphene*, *Nature (London)* **590**, 249 (2021).

- [98] J. W. F. Venderbos and R. M. Fernandes, *Correlations and electronic order in a two-orbital honeycomb lattice model for twisted bilayer graphene*, *Phys. Rev. B* **98**, 245103 (2018).
- [99] J. F. Dodaro, S. A. Kivelson, Y. Schattner, X. Q. Sun, and C. Wang, *Phases of a phenomenological model of twisted bilayer graphene*, *Phys. Rev. B* **98**, 075154 (2018).
- [100] H. C. Po, L. Zou, A. Vishwanath, and T. Senthil, *Origin of Mott insulating behavior and superconductivity in twisted bilayer graphene*, *Phys. Rev. X* **8**, 031089 (2018).
- [101] N. F. Q. Yuan and L. Fu, *Model for the metal-insulator transition in graphene superlattices and beyond*, *Phys. Rev. B* **98**, 045103 (2018).
- [102] L. Balents, C. R. Dean, D. K. Efetov, and A. F. Young, *Superconductivity and strong correlations in moiré flat bands*, *Nat. Phys.* **16**, 725 (2020).
- [103] B. A. Bernevig, B. Lian, A. Cowsik, F. Xie, N. Regnault, and Z.-D. Song, *Twisted bilayer graphene. V. Exact analytic many-body excitations in Coulomb Hamiltonians: Charge gap, Goldstone modes, and absence of Cooper pairing*, *Phys. Rev. B* **103**, 205415 (2021).
- [104] R. M. Fernandes and L. Fu, *Charge-4e superconductivity from multicomponent nematic pairing: Application to twisted bilayer graphene*, *Phys. Rev. Lett.* **127**, 047001 (2021).
- [105] F. Wu, E. Hwang, and S. Das Sarma, *Phonon-induced giant linear-in-T resistivity in magic angle twisted bilayer graphene: Ordinary strangeness and exotic superconductivity*, *Phys. Rev. B* **99**, 165112 (2019).
- [106] F. Xie, Z. Song, B. Lian, and B. A. Bernevig, *Topology-bounded superfluid weight in twisted bilayer graphene*, *Phys. Rev. Lett.* **124**, 167002 (2020).
- [107] R. M. Fernandes and J. W. F. Venderbos, *Nematicity with a twist: Rotational symmetry breaking in a moiré superlattice*, *Sci. Adv.* **6**, eaba8834 (2020).
- [108] A. Blason and M. Fabrizio, *Local Kekulé distortion turns twisted bilayer graphene into topological Mott insulators and superconductors*, *Phys. Rev. B* **106**, 235112 (2022).
- [109] M. Angeli, E. Tosatti, and M. Fabrizio, *Valley Jahn-Teller effect in twisted bilayer graphene*, *Phys. Rev. X* **9**, 041010 (2019).
- [110] J. H. Pixley and E. Y. Andrei, *Ferromagnetism in magic-angle graphene*, *Science* **365**, 543 (2019).
- [111] J. Liu and X. Dai, *Anomalous Hall effect, magneto-optical properties, and nonlinear optical properties of twisted graphene systems*, *npj Comput. Mater.* **6**, 1 (2020).
- [112] L. Zou, H. C. Po, A. Vishwanath, and T. Senthil, *Band structure of twisted bilayer graphene: Emergent symmetries, commensurate approximants, and Wannier obstructions*, *Phys. Rev. B* **98**, 085435 (2018).
- [113] H. C. Po, H. Watanabe, and A. Vishwanath, *Fragile topology and Wannier obstructions*, *Phys. Rev. Lett.* **121**, 126402 (2018).
- [114] K. Hejazi, C. Liu, and L. Balents, *Landau levels in twisted bilayer graphene and semiclassical orbits*, *Phys. Rev. B* **100**, 035115 (2019).
- [115] J. Ahn, S. Park, and B.-J. Yang, *Failure of Nielsen-Ninomiya theorem and fragile topology in two-dimensional systems with space-time inversion symmetry: Application to twisted bilayer graphene at magic angle*, *Phys. Rev. X* **9**, 021013 (2019).
- [116] H. C. Po, L. Zou, T. Senthil, and A. Vishwanath, *Faithful tight-binding models and fragile topology of magic-angle bilayer graphene*, *Phys. Rev. B* **99**, 195455 (2019).
- [117] Z. Song, Z. Wang, W. Shi, G. Li, C. Fang, and B. A. Bernevig, *All magic angles in twisted bilayer graphene are topological*, *Phys. Rev. Lett.* **123**, 036401 (2019).
- [118] J. Liu, Z. Ma, J. Gao, and X. Dai, *Quantum valley Hall effect, orbital magnetism, and anomalous Hall effect in twisted multilayer graphene systems*, *Phys. Rev. X* **9**, 031021 (2019).
- [119] Z.-D. Song, B. Lian, N. Regnault, and B. A. Bernevig, *Twisted bilayer graphene. II. Stable symmetry anomaly*, *Phys. Rev. B* **103**, 205412 (2021).
- [120] J. Herzog-Arbeitman, Z.-D. Song, N. Regnault, and B. A. Bernevig, *Hofstadter topology: Noncrystalline topological materials at high flux*, *Phys. Rev. Lett.* **125**, 236804 (2020).
- [121] J. Wang, Y. Zheng, A. J. Millis, and J. Cano, *Chiral approximation to twisted bilayer graphene: Exact intra-valley inversion symmetry, nodal structure, and implications for higher magic angles*, *Phys. Rev. Res.* **3**, 023155 (2021).
- [122] S. Dai, Y. Xiang, and D. J. Srolovitz, *Twisted bilayer graphene: Moiré with a twist*, *Nano Lett.* **16**, 5923 (2016).
- [123] S. K. Jain, V. Juričić, and G. T. Barkema, *Structure of twisted and buckled bilayer graphene*, *2D Mater.* **4**, 015018 (2016).
- [124] K. Uchida, S. Furuya, J.-I. Iwata, and A. Oshiyama, *Atomic corrugation and electron localization due to moiré patterns in twisted bilayer graphenes*, *Phys. Rev. B* **90**, 155451 (2014).
- [125] M. M. van Wijk, A. Schuring, M. I. Katsnelson, and A. Fasolino, *Relaxation of moiré patterns for slightly misaligned identical lattices: Graphene on graphite*, *2D Mater.* **2**, 034010 (2015).
- [126] P. Moon and M. Koshino, *Optical absorption in twisted bilayer graphene*, *Phys. Rev. B* **87**, 205404 (2013).
- [127] J. Kang and O. Vafek, *Symmetry, maximally localized Wannier states, and a low-energy model for twisted bilayer graphene narrow bands*, *Phys. Rev. X* **8**, 031088 (2018).
- [128] S. Carr, S. Fang, Z. Zhu, and E. Kaxiras, *Exact continuum model for low-energy electronic states of twisted bilayer graphene*, *Phys. Rev. Res.* **1**, 013001 (2019).
- [129] S. Fang, S. Carr, Z. Zhu, D. Massatt, and E. Kaxiras, *Angle-dependent ab initio low-energy Hamiltonians for a relaxed twisted bilayer graphene heterostructure*, *arXiv:1908.00058*.
- [130] G. Tarnopolsky, A. J. Kruchkov, and A. Vishwanath, *Origin of magic angles in twisted bilayer graphene*, *Phys. Rev. Lett.* **122**, 106405 (2019).
- [131] D. K. Efimkin and A. H. MacDonald, *Helical network model for twisted bilayer graphene*, *Phys. Rev. B* **98**, 035404 (2018).
- [132] M. Koshino, N. F. Q. Yuan, T. Koretsune, M. Ochi, K. Kuroki, and L. Fu, *Maximally localized Wannier orbitals and the extended Hubbard model for twisted bilayer graphene*, *Phys. Rev. X* **8**, 031087 (2018).

- [133] Y.-H. Zhang, D. Mao, Y. Cao, P. Jarillo-Herrero, and T. Senthil, *Nearly flat Chern bands in moiré superlattices*, *Phys. Rev. B* **99**, 075127 (2019).
- [134] Y. Huang, P. Hosur, and H. K. Pal, *Quasi-flat-band physics in a two-leg ladder model and its relation to magic-angle twisted bilayer graphene*, *Phys. Rev. B* **102**, 155429 (2020).
- [135] J.H. Wilson, Y. Fu, S. Das Sarma, and J.H. Pixley, *Disorder in twisted bilayer graphene*, *Phys. Rev. Res.* **2**, 023325 (2020).
- [136] Y. Fu, E.J. König, J.H. Wilson, Y.-Z. Chou, and J.H. Pixley, *Magic-angle semimetals*, *npj Quantum Mater.* **5**, 1 (2020).
- [137] B. Padhi, A. Tiwari, T. Neupert, and S. Ryu, *Transport across twist angle domains in moiré graphene*, *Phys. Rev. Res.* **2**, 033458 (2020).
- [138] O. Vafek and J. Kang, *Lattice model for the Coulomb interacting chiral limit of magic-angle twisted bilayer graphene: Symmetries, obstructions, and excitations*, *Phys. Rev. B* **104**, 075143 (2021).
- [139] B. A. Bernevig, Z.-D. Song, N. Regnault, and B. Lian, *Twisted bilayer graphene. I. Matrix elements, approximations, perturbation theory, and a $k \cdot p$ two-band model*, *Phys. Rev. B* **103**, 205411 (2021).
- [140] B. A. Bernevig, Z.-D. Song, N. Regnault, and B. Lian, *Twisted bilayer graphene. III. Interacting Hamiltonian and exact symmetries*, *Phys. Rev. B* **103**, 205413 (2021).
- [141] K. Hejazi, X. Chen, and L. Balents, *Hybrid Wannier Chern bands in magic angle twisted bilayer graphene and the quantized anomalous Hall effect*, *Phys. Rev. Res.* **3**, 013242 (2021).
- [142] J. Cao, M. Wang, S.-F. Qian, C.-C. Liu, and Y. Yao, *Ab initio four-band Wannier tight-binding model for generic twisted graphene systems*, *Phys. Rev. B* **104**, L081403 (2021).
- [143] Y.-Z. Chou and S. Das Sarma, *Kondo lattice model in magic-angle twisted bilayer graphene*, *Phys. Rev. Lett.* **131**, 026501 (2023).
- [144] A. Davydov, K. Choo, M.H. Fischer, and T. Neupert, *Construction of low-energy symmetric Hamiltonians and Hubbard parameters for twisted multilayer systems using ab initio input*, *Phys. Rev. B* **105**, 165153 (2022).
- [145] H. Shi and X. Dai, *Heavy-fermion representation for twisted bilayer graphene systems*, *Phys. Rev. B* **106**, 245129 (2022).
- [146] X. Wang, J. Finney, A. L. Sharpe, L. K. Rodenbach, C. L. Hsueh, K. Watanabe, T. Taniguchi, M. A. Kastner, O. Vafek, and D. Goldhaber-Gordon, *Unusual magnetotransport in twisted bilayer graphene from strain-induced open Fermi surfaces*, *Proc. Natl. Acad. Sci. U.S.A.* **120**, e2307151120 (2023).
- [147] L. L. H. Lau and P. Coleman, *Topological mixed valence model for twisted bilayer graphene*, [arXiv:2303.02670](https://arxiv.org/abs/2303.02670).
- [148] Y. Li, B. M. Fregoso, and M. Dzero, *Topological mixed valence model in magic-angle twisted bilayer graphene*, *Phys. Rev. B* **110**, 045123 (2024).
- [149] D. M. Kennes, M. Claassen, L. Xian, A. Georges, A. J. Millis, J. Hone, C. R. Dean, D. N. Basov, A. N. Pasupathy, and A. Rubio, *Moiré heterostructures as a condensed-matter quantum simulator*, *Nat. Phys.* **17**, 155 (2021).
- [150] E. Y. Andrei, D. K. Efetov, P. Jarillo-Herrero, A. H. MacDonald, K. F. Mak, T. Senthil, E. Tutuc, A. Yazdani, and A. F. Young, *The marvels of moiré materials*, *Nat. Rev. Mater.* **6**, 201 (2021).
- [151] Y. Cao, D. Chowdhury, D. Rodan-Legrain, O. Rubies-Bigorda, K. Watanabe, T. Taniguchi, T. Senthil, and P. Jarillo-Herrero, *Strange metal in magic-angle graphene with near Planckian dissipation*, *Phys. Rev. Lett.* **124**, 076801 (2020).
- [152] P. Stepanov, I. Das, X. Lu, A. Fahimniya, K. Watanabe, T. Taniguchi, F. H. L. Koppens, J. Lischner, L. Levitov, and D. K. Efetov, *Untying the insulating and superconducting orders in magic-angle graphene*, *Nature (London)* **583**, 375 (2020).
- [153] M. Xie and A. H. MacDonald, *Weak-field Hall resistivity and spin-valley flavor symmetry breaking in magic-angle twisted bilayer graphene*, *Phys. Rev. Lett.* **127**, 196401 (2021).
- [154] A. Kerelsky, L. J. McGilly, D. M. Kennes, L. Xian, M. Yankowitz, S. Chen, K. Watanabe, T. Taniguchi, J. Hone, C. Dean, A. Rubio, and A. N. Pasupathy, *Maximized electron interactions at the magic angle in twisted bilayer graphene*, *Nature (London)* **572**, 95 (2019).
- [155] Y. Jiang, X. Lai, K. Watanabe, T. Taniguchi, K. Haule, J. Mao, and E. Y. Andrei, *Charge order and broken rotational symmetry in magic-angle twisted bilayer graphene*, *Nature (London)* **573**, 91 (2019).
- [156] D. Wong, K. P. Nuckolls, M. Oh, B. Lian, Y. Xie, S. Jeon, K. Watanabe, T. Taniguchi, B. A. Bernevig, and A. Yazdani, *Cascade of electronic transitions in magic-angle twisted bilayer graphene*, *Nature (London)* **582**, 198 (2020).
- [157] I. Das, X. Lu, J. Herzog-Arbeitman, Z.-D. Song, K. Watanabe, T. Taniguchi, B. A. Bernevig, and D. K. Efetov, *Symmetry-broken Chern insulators and Rashba-like Landau-level crossings in magic-angle bilayer graphene*, *Nat. Phys.* **17**, 710 (2021).
- [158] Y. Choi, H. Kim, Y. Peng, A. Thomson, C. Lewandowski, R. Polski, Y. Zhang, H. S. Arora, K. Watanabe, T. Taniguchi, J. Alicea, and S. Nadj-Perge, *Correlation-driven topological phases in magic-angle twisted bilayer graphene*, *Nature (London)* **589**, 536 (2021).
- [159] Y. Choi, H. Kim, C. Lewandowski, Y. Peng, A. Thomson, R. Polski, Y. Zhang, K. Watanabe, T. Taniguchi, J. Alicea, and S. Nadj-Perge, *Interaction-driven band flattening and correlated phases in twisted bilayer graphene*, *Nat. Phys.* **17**, 1375 (2021).
- [160] Y. Choi, H. Kim, Y. Peng, A. Thomson, C. Lewandowski, R. Polski, Y. Zhang, H. S. Arora, K. Watanabe, T. Taniguchi, J. Alicea, and S. Nadj-Perge, *Correlation-driven topological phases in magic-angle twisted bilayer graphene*, *Nature (London)* **589**, 536 (2021).
- [161] J. M. Park, Y. Cao, K. Watanabe, T. Taniguchi, and P. Jarillo-Herrero, *Flavour Hund's coupling, Chern gaps and charge diffusivity in moiré graphene*, *Nature (London)* **592**, 43 (2021).
- [162] X. Lu, B. Lian, G. Chaudhary, B. A. Piot, G. Romagnoli, K. Watanabe, T. Taniguchi, M. Poggio, A. H. MacDonald, B. A. Bernevig, and D. K. Efetov, *Multiple flat bands and topological Hofstadter butterfly in twisted bilayer*

- graphene close to the second magic angle*, *Proc. Natl. Acad. Sci. U.S.A.* **118**, e2100006118 (2021).
- [163] A. Rozen, J. M. Park, U. Zondiner, Y. Cao, D. Rodan-Legrain, T. Taniguchi, K. Watanabe, Y. Oreg, A. Stern, E. Berg, P. Jarillo-Herrero, and S. Ilani, *Entropic evidence for a Pomeranchuk effect in magic-angle graphene*, *Nature (London)* **592**, 214 (2021).
- [164] Y. Saito, F. Yang, J. Ge, X. Liu, T. Taniguchi, K. Watanabe, J. I. A. Li, E. Berg, and A. F. Young, *Isospin Pomeranchuk effect in twisted bilayer graphene*, *Nature (London)* **592**, 220 (2021).
- [165] I. Das, C. Shen, A. Jaoui, J. Herzog-Arbeitman, A. Chew, C.-W. Cho, K. Watanabe, T. Taniguchi, B. A. Piot, B. A. Bernevig, and D. K. Efetov, *Observation of reentrant correlated insulators and interaction-driven Fermi-surface reconstructions at one magnetic flux quantum per moiré unit cell in magic-angle twisted bilayer graphene*, *Phys. Rev. Lett.* **128**, 217701 (2022).
- [166] P. Seifert, X. Lu, P. Stepanov, J. R. Durán Retamal, J. N. Moore, K.-C. Fong, A. Principi, and D. K. Efetov, *Magic-angle bilayer graphene nanocalorimeters: Toward broadband, energy-resolving single photon detection*, *Nano Lett.* **20**, 3459 (2020).
- [167] M. Otteneder, S. Hubmann, X. Lu, D. A. Kozlov, L. E. Golub, K. Watanabe, T. Taniguchi, D. K. Efetov, and S. D. Ganichev, *Terahertz photogalvanics in twisted bilayer graphene close to the second magic angle*, *Nano Lett.* **20**, 7152 (2020).
- [168] S. Lisi, X. Lu, T. Benschop, T. A. de Jong, P. Stepanov, J. R. Duran, F. Margot, I. Cucchi, E. Cappelli, A. Hunter *et al.*, *Observation of flat bands in twisted bilayer graphene*, *Nat. Phys.* **17**, 189 (2021).
- [169] T. Benschop, T. A. de Jong, P. Stepanov, X. Lu, V. Stalman, S. J. van der Molen, D. K. Efetov, and M. P. Allan, *Measuring local moiré lattice heterogeneity of twisted bilayer graphene*, *Phys. Rev. Res.* **3**, 013153 (2021).
- [170] N. C. H. Hesp, I. Torre, D. Rodan-Legrain, P. Novelli, Y. Cao, S. Carr, S. Fang, P. Stepanov, D. Barcons-Ruiz, H. Herzig Sheinflux, K. Watanabe, T. Taniguchi, D. K. Efetov, E. Kaxiras, P. Jarillo-Herrero, M. Polini, and F. H. L. Koppens, *Observation of interband collective excitations in twisted bilayer graphene*, *Nat. Phys.* **17**, 1162 (2021).
- [171] S. Hubmann, P. Soul, G. Di Battista, M. Hild, K. Watanabe, T. Taniguchi, D. K. Efetov, and S. D. Ganichev, *Nonlinear intensity dependence of photogalvanics and photoconductance induced by terahertz laser radiation in twisted bilayer graphene close to magic angle*, *Phys. Rev. Mater.* **6**, 024003 (2022).
- [172] S. Grover, M. Bocarsly, A. Uri, P. Stepanov, G. Di Battista, I. Roy, J. Xiao, A. Y. Meltzer, Y. Myasoedov, K. Pareek, K. Watanabe, T. Taniguchi, B. Yan, A. Stern, E. Berg, D. K. Efetov, and E. Zeldov, *Chern mosaic and Berry-curvature magnetism in magic-angle graphene*, *Nat. Phys.* **18**, 885 (2022).
- [173] Y. Choi, J. Kemmer, Y. Peng, A. Thomson, H. Arora, R. Polski, Y. Zhang, H. Ren, J. Alicea, G. Refael, F. von Oppen, K. Watanabe, T. Taniguchi, and S. Nadj-Perge, *Electronic correlations in twisted bilayer graphene near the magic angle*, *Nat. Phys.* **15**, 1174 (2019).
- [174] C. L. Tschirhart, M. Serlin, H. Polshyn, A. Shragai, Z. Xia, J. Zhu, Y. Zhang, K. Watanabe, T. Taniguchi, M. E. Huber, and A. F. Young, *Imaging orbital ferromagnetism in a moiré Chern insulator*, *Science* **372**, 1323 (2021).
- [175] Y. Xie, B. Lian, B. Jäck, X. Liu, C.-L. Chiu, K. Watanabe, T. Taniguchi, B. A. Bernevig, and A. Yazdani, *Spectroscopic signatures of many-body correlations in magic-angle twisted bilayer graphene*, *Nature (London)* **572**, 101 (2019).
- [176] D. Călugăru, M. Borovkov, L. L. H. Lau, P. Coleman, Z.-D. Song, and B. A. Bernevig, *Twisted bilayer graphene as topological heavy fermion: II. Analytical approximations of the model parameters*, *Low Temp. Phys.* **49**, 640 (2023).
- [177] X. Liu, Z. Wang, K. Watanabe, T. Taniguchi, O. Vafek, and J. I. A. Li, *Tuning electron correlation in magic-angle twisted bilayer graphene using Coulomb screening*, *Science* **371**, 1261 (2021).
- [178] Y. Saito, J. Ge, L. Rademaker, K. Watanabe, T. Taniguchi, D. A. Abanin, and A. F. Young, *Hofstadter subband ferromagnetism and symmetry-broken Chern insulators in twisted bilayer graphene*, *Nat. Phys.* **17**, 478 (2021).
- [179] Y. Cao, D. Rodan-Legrain, J. M. Park, N. F. Q. Yuan, K. Watanabe, T. Taniguchi, R. M. Fernandes, L. Fu, and P. Jarillo-Herrero, *Nematicity and competing orders in superconducting magic-angle graphene*, *Science* **372**, 264 (2021).
- [180] J. Yu, B. A. Foutty, Z. Han, M. E. Barber, Y. Schattner, K. Watanabe, T. Taniguchi, P. Phillips, Z.-X. Shen, S. A. Kivelson, and B. E. Feldman, *Correlated Hofstadter spectrum and flavour phase diagram in magic-angle twisted bilayer graphene*, *Nat. Phys.* **18**, 825 (2022).
- [181] K. P. Nuckolls, R. L. Lee, M. Oh, D. Wong, T. Soejima, J. P. Hong, D. Călugăru, J. Herzog-Arbeitman, B. A. Bernevig, K. Watanabe, T. Taniguchi, N. Regnault, M. P. Zaletel, and A. Yazdani, *Quantum textures of the many-body wavefunctions in magic-angle graphene*, *Nature (London)* **620**, 525 (2023).
- [182] A. Georges, G. Kotliar, W. Krauth, and M. J. Rozenberg, *Dynamical mean-field theory of strongly correlated fermion systems and the limit of infinite dimensions*, *Rev. Mod. Phys.* **68**, 13 (1996).
- [183] W. Metzner and D. Vollhardt, *Correlated lattice fermions in $d = \infty$ dimensions*, *Phys. Rev. Lett.* **62**, 324 (1989).
- [184] A. Georges and G. Kotliar, *Hubbard model in infinite dimensions*, *Phys. Rev. B* **45**, 6479 (1992).
- [185] M. Haule, E. Y. Andrei, and K. Haule, *The Mott-semiconducting state in the magic angle bilayer graphene*, [arXiv:1901.09852](https://arxiv.org/abs/1901.09852).
- [186] A. Datta, M. J. Calderón, A. Camjayi, and E. Bascones, *Heavy quasiparticles and cascades without symmetry breaking in twisted bilayer graphene*, *Nat. Commun.* **14**, 5036 (2023).
- [187] A. A. Katanin, *Charge and spin correlations in insulating and incoherent metal states of twisted bilayer graphene*, *Phys. Rev. B* **106**, 115147 (2022).
- [188] H. Hu, G. Rai, L. Crippa, J. Herzog-Arbeitman, D. Călugăru, T. Wehling, G. Sangiovanni, R. Valentí, A. M. Tsvelik, and B. A. Bernevig, *Symmetric Kondo lattice states in doped strained twisted bilayer graphene*, *Phys. Rev. Lett.* **131**, 166501 (2023).

- [189] G.-D. Zhou, Y.-J. Wang, N. Tong, and Z.-D. Song, *Kondo phase in twisted bilayer graphene*, *Phys. Rev. B* **109**, 045419 (2024).
- [190] S. L. Tomarken, Y. Cao, A. Demir, K. Watanabe, T. Taniguchi, P. Jarillo-Herrero, and R. C. Ashoori, *Electronic compressibility of magic-angle graphene superlattices*, *Phys. Rev. Lett.* **123**, 046601 (2019).
- [191] A. T. Pierce, Y. Xie, J. M. Park, E. Khalaf, S. H. Lee, Y. Cao, D. E. Parker, P. R. Forrester, S. Chen, K. Watanabe, T. Taniguchi, A. Vishwanath, P. Jarillo-Herrero, and A. Yacoby, *Unconventional sequence of correlated Chern insulators in magic-angle twisted bilayer graphene*, *Nat. Phys.* **17**, 1210 (2021).
- [192] C. Shen, Y. Chu, Q. Wu, N. Li, S. Wang, Y. Zhao, J. Tang, J. Liu, J. Tian, K. Watanabe, T. Taniguchi, R. Yang, Z. Y. Meng, D. Shi, O. V. Yazyev, and G. Zhang, *Correlated states in twisted double bilayer graphene*, *Nat. Phys.* **16**, 520 (2020).
- [193] A. Inbar, J. Birkbeck, J. Xiao, T. Taniguchi, K. Watanabe, B. Yan, Y. Oreg, A. Stern, E. Berg, and S. Ilani, *The quantum twisting microscope*, *Nature (London)* **614**, 682 (2023).
- [194] U. Zondiner, A. Rozen, D. Rodan-Legrain, Y. Cao, R. Queiroz, T. Taniguchi, K. Watanabe, Y. Oreg, F. von Oppen, A. Stern, E. Berg, P. Jarillo-Herrero, and S. Ilani, *Cascade of phase transitions and Dirac revivals in magic-angle graphene*, *Nature (London)* **582**, 203 (2020).
- [195] I. Pomeranchuk, *On the theory of liquid 3 – He*, *Zh. Eksp. Teor. Fiz.* **20**, 919 (1950).
- [196] A. Georges and W. Krauth, *Numerical solution of the $d = \infty$ Hubbard model: Evidence for a Mott transition*, *Phys. Rev. Lett.* **69**, 1240 (1992).
- [197] A. Georges and W. Krauth, *Physical properties of the half-filled Hubbard model in infinite dimensions*, *Phys. Rev. B* **48**, 7167 (1993).
- [198] F. Werner, O. Parcollet, A. Georges, and S. R. Hassan, *Interaction-induced adiabatic cooling and antiferromagnetism of cold fermions in optical lattices*, *Phys. Rev. Lett.* **95**, 056401 (2005).
- [199] S. Taie, R. Yamazaki, S. Sugawa, and Y. Takahashi, *An $Su(6)$ Mott insulator of an atomic Fermi gas realized by large-spin pomeranchuk cooling*, *Nat. Phys.* **8**, 825 (2012).
- [200] H. Hu, B. A. Bernevig, and A. M. Tsvelik, *Kondo lattice model of magic-angle twisted-bilayer graphene: Hund's rule, local-moment fluctuations, and low-energy effective theory*, *Phys. Rev. Lett.* **131**, 026502 (2023).
- [201] J. P. Eisenstein, L. N. Pfeiffer, and K. W. West, *Negative compressibility of interacting two-dimensional electron and quasiparticle gases*, *Phys. Rev. Lett.* **68**, 674 (1992).
- [202] J. M. Riley, W. Meevasana, L. Bawden, M. Asakawa, T. Takayama, T. Eknapakul, T. K. Kim, M. Hoesch, S.-K. Mo, H. Takagi, T. Sasagawa, M. S. Bahramy, and P. D. C. King, *Negative electronic compressibility and tunable spin splitting in WSe_2* , *Nat. Nanotechnol.* **10**, 1043 (2015).
- [203] A. M. J. Schakel, *Ground state of electron gases at negative compressibility*, *Phys. Rev. B* **64**, 245101 (2001).
- [204] See Supplemental Material at <http://link.aps.org/supplemental/10.1103/PhysRevX.14.031045> for the full Hamiltonian, the technical details of the DMFT and Hartree-Fock calculations, the procedure to subtract the geometric capacitance, and a movie showing the evolution of the spectral weight in twisted bilayer graphene.
- [205] O. Parcollet, M. Ferrero, T. Ayril, H. Hafermann, I. Krivenko, L. Messio, and P. Seth, *TRIQS: A toolbox for research on interacting quantum systems*, *Comput. Phys. Commun.* **196**, 398 (2015).
- [206] P. Seth, I. Krivenko, M. Ferrero, and O. Parcollet, *TRIQS/CTHYB: A continuous-time quantum Monte Carlo hybridization expansion solver for quantum impurity problems*, *Comput. Phys. Commun.* **200**, 274 (2016).
- [207] M. Aichhorn, L. Pourovskii, P. Seth, V. Vildosola, M. Zingl, O. E. Peil, X. Deng, J. Mravlje, G. J. Kraberger, C. Martins, M. Ferrero, and O. Parcollet, *TRIQS/DFTTools: A TRIQS application for ab initio calculations of correlated materials*, *Comput. Phys. Commun.* **204**, 200 (2016).
- [208] N. Parragh, A. Toschi, K. Held, and G. Sangiovanni, *Conserved quantities of $SU(2)$ -invariant interactions for correlated fermions and the advantages for quantum Monte Carlo simulations*, *Phys. Rev. B* **86**, 155158 (2012).
- [209] M. Wallerberger, A. Hausoel, P. Gunacker, A. Kowalski, N. Parragh, F. Goth, K. Held, and G. Sangiovanni, *w2DYNAMICS: Local one- and two-particle quantities from dynamical mean field theory*, *Comput. Phys. Commun.* **235**, 388 (2019).
- [210] J. E. Gubernatis, M. Jarrell, R. N. Silver, and D. S. Sivia, *Quantum Monte Carlo simulations and maximum entropy: Dynamics from imaginary-time data*, *Phys. Rev. B* **44**, 6011 (1991).
- [211] G. J. Kraberger, R. Triebl, M. Zingl, and M. Aichhorn, *Maximum entropy formalism for the analytic continuation of matrix-valued Green's functions*, *Phys. Rev. B* **96**, 155128 (2017).
- [212] J. Kaufmann and K. Held, *ana_cont: PYTHON package for analytic continuation*, arXiv:2105.11211.
- [213] <https://github.com/lcrippa/w2dynamics-matbg-symmetric>, https://github.com/gautamra/TBLG_ordered.
- [214] G. Rai, L. Crippa, G. Sangiovanni, and T. O. Wehling, *Figure data for dynamical correlations and order in magic-angle twisted bilayer graphene (1.0)*, Zenodo (2024), [10.5281/zenodo.13378388](https://zenodo.org/record/13378388).
- [215] G. Sangiovanni, A. Toschi, E. Koch, K. Held, M. Capone, C. Castellani, O. Gunnarsson, S.-K. Mo, J. W. Allen, H.-D. Kim, A. Sekiyama, A. Yamasaki, S. Suga, and P. Metcalf, *Static versus dynamical mean-field theory of Mott antiferromagnets*, *Phys. Rev. B* **73**, 205121 (2006).
- [216] Y.-Z. Chou and S. Das Sarma, *Scaling theory of intrinsic Kondo and Hund's rule interactions in magic-angle twisted bilayer graphene*, *Phys. Rev. B* **108**, 125106 (2023).
- [217] M. Imada, A. Fujimori, and Y. Tokura, *Metal-insulator transitions*, *Rev. Mod. Phys.* **70**, 1039 (1998).
- [218] A. Amaricci, L. de' Medici, and M. Capone, *Mott transitions with partially filled correlated orbitals*, *Europhys. Lett.* **118**, 17004 (2017).
- [219] L. de' Medici, A. Georges, G. Kotliar, and S. Biermann, *Mott transition and Kondo screening in f -electron metals*, *Phys. Rev. Lett.* **95**, 066402 (2005).
- [220] D. Călugăru *et al.* (to be published).
- [221] P. Pulay, *Convergence acceleration of iterative sequences. The case of scf iteration*, *Chem. Phys. Lett.* **73**, 393 (1980).

- [222] J. Kang, B. A. Bernevig, and O. Vafek, *Cascades between light and heavy fermions in the normal state of magic angle twisted bilayer graphene*, *Phys. Rev. Lett.* **127**, 266402 (2021).
- [223] P. B. Allen, H. Berger, O. Chauvet, L. Forro, T. Jarlborg, A. Junod, B. Revaz, and G. Santi, *Transport properties, thermodynamic properties, and electronic structure of SrRuO₃*, *Phys. Rev. B* **53**, 4393 (1996).
- [224] M. Edelmann, G. Sangiovanni, M. Capone, and L. de' Medici, *Chromium analogs of iron-based superconductors*, *Phys. Rev. B* **95**, 205118 (2017).
- [225] A. Georges, G. Kotliar, and W. Krauth, *Superconductivity in the two-band Hubbard model in infinite dimensions*, *Z. Phys. B* **92**, 313 (1993).
- [226] V. I. Anisimov, J. Zaanen, and O. K. Andersen, *Band theory and Mott insulators: Hubbard U instead of Stoner I* , *Phys. Rev. B* **44**, 943 (1991).
- [227] I. V. Solovyev, P. H. Dederichs, and V. I. Anisimov, *Corrected atomic limit in the local-density approximation and the electronic structure of d impurities in Rb*, *Phys. Rev. B* **50**, 16861 (1994).
- [228] M. T. Czyżyk and G. A. Sawatzky, *Local-density functional and on-site correlations: The electronic structure of La₂CuO₄ and LaCuO₃*, *Phys. Rev. B* **49**, 14211 (1994).
- [229] T. Kopp and J. Mannhart, *Calculation of the capacitances of conductors: Perspectives for the optimization of electronic devices*, *J. Appl. Phys.* **106**, 064504 (2009).
- [230] L. Li, C. Richter, S. Paetel, T. Kopp, J. Mannhart, and R. C. Ashoori, *Very large capacitance enhancement in a two-dimensional electron system*, *Science* **332**, 825 (2011).
- [231] T. Kopp and J. Mannhart, *Calculation of the capacitances of conductors: Perspectives for the optimization of electronic devices*, *J. Appl. Phys.* **106**, 064504 (2009).
- [232] J. Herzog-Arbeitman, J. Yu, D. Călugăru, H. Hu, N. Regnault, O. Vafek, J. Kang, and B. A. Bernevig, *Heavy fermions as an efficient representation of atomistic strain and relaxation in twisted bilayer graphene*, [arXiv:2405.13880](https://arxiv.org/abs/2405.13880).